

# Stability of flat-band Bose-Einstein condensation from the geometry of compact localized states

Kukka-Emilia Huhtinen\*

*Institute for Theoretical Physics, ETH Zurich, 8093 Zürich, Switzerland*

(Dated: March 11, 2026)

We consider Bose-Einstein condensation in flat-band models from a real-space perspective. Using a basis of compact localized states, we reformulate the minimization of the mean-field energy as a Euclidian geometry problem. Within Bogoliubov theory, we show that flat-band models where the solutions to this problem are frameworks consisting of triangles with nonzero area are promising for condensation, whereas for instance square frameworks indicate condensation in a single mode is impossible. When restricting the analysis to Bloch states, this approach can be related to a necessary condition for a non-vanishing quantum distance. This work provides a new perspective on how condensation in flat bands is destabilized, and offers principles for the construction of models where flat-band Bose-Einstein condensation is possible.

## I. INTRODUCTION

Flat bands have attracted increased interest in recent years because correlated phenomena are often enhanced in the absence of kinetic energy [1–3]. Naively, the infinite effective mass of single particles might seem to present a problem for phenomena such as superconductivity, but physical properties in multiband models are affected by not only the band dispersion, but also the geometry of quantum states. Of particular importance for flat-band properties is the quantum metric [4] and its basis-invariant generalizations, which can appear for instance in the superfluid weight [1, 5–7] and other electromagnetic responses [8–15].

One interesting question is how the degeneracy of flat-band states affects the properties of bosonic systems, and especially the possibility of Bose-Einstein condensation. Bosonic flat-band systems have been studied experimentally in various platforms [16–28], and previous theoretical research has indicated that some models such as the kagome lattice can host a condensate for large enough densities [29–31], while others can not. Quantum geometry gives a beginning of an answer regarding the stability of flat-band condensates and superfluids: the quantum distance and the quantum metric play an important role. The former is involved in the excitation fraction [32–34], while the latter can determine the speed of sound [32–35], the effective mass of superfluid carriers [36] and part of the superfluid weight [37]. A momentum-space approach requires several assumptions, however: for instance, condensation is typically assumed to occur in a Bloch state, which might not always be the case in a flat band. To verify this assumption, a real-space approach, such as the one used in Ref. 30 for the kagome lattice, is typically necessary.

Here, we adopt a related approach for generic tight-binding flat-band models, relying on the existence of compact localized states (CLSs). CLSs are single-particle flat-band eigenstates localized in real space by destructive interference [38–40], and give insight, for instance,

on band touchings between flat and dispersive bands [41–43]. CLSs have been observed in various flat band systems [16, 17, 21, 44–56], and can be used as a starting point for the construction of flat band models [44, 57–66].

In this work, we show how the properties of CLSs, i.e. eigenstates of the non-interacting Hamiltonian, impact whether bosons can condense once interactions are included. In this sense, the method is similar in spirit to the usual quantum geometric approach, which relates properties of an interacting system to the geometry of Bloch states. However, the two approaches are not equivalent, but rather complementary. The method proposed here considers all flat-band states instead of only Bloch states, and because CLSs are a convenient starting point in the construction of flat band models, offers principles for designing flat bands with stable Bose-Einstein condensation.

## II. BOGOLIUBOV THEORY ON A FLAT BAND

We consider the Bose-Hubbard Hamiltonian on a multi-band lattice,  $H = H_{\text{kin}} + H_{\text{int}}$ , where

$$\begin{aligned} H_{\text{kin}} &= \sum_{i\alpha, j\beta} b_{i\alpha}^\dagger t_{i\alpha, j\beta} b_{j\beta}, \\ H_{\text{int}} &= \frac{U}{2} \sum_{i\alpha} n_{i\alpha} (n_{i\alpha} - 1) - \mu \sum_{i\alpha} n_{i\alpha}. \end{aligned} \quad (1)$$

Here,  $b_{i\alpha}^\dagger$  creates a boson at orbital  $\alpha$  in the  $i$ th unit cell, and  $n_{i\alpha} = b_{i\alpha}^\dagger b_{i\alpha}$ . The bosons can hop from site  $j\beta$  to  $i\alpha$  with amplitude  $t_{i\alpha, j\beta}$ , and  $t_{i\alpha, i\alpha}$  is the on-site potential at  $i\alpha$ . Particles experience an on-site repulsive interaction  $U$ , and  $\mu$  is the chemical potential.

We assume condensation in a single flat-band eigenstate  $|\varphi_0\rangle$  such that  $H_{\text{kin}} |\varphi_0\rangle = \varepsilon_0 |\varphi_0\rangle$ , where  $\varepsilon_0$  is the flat-band energy, and study the stability of the condensate within Bogoliubov theory. The state  $|\varphi_0\rangle$  does not need to be a Bloch state. We expand  $b_{i\alpha} = \sqrt{N_0} \varphi_{i\alpha} + c_{i\alpha}$ , where  $\varphi_{i\alpha} \equiv |\varphi_0(\mathbf{r}_{i\alpha})\rangle$  with  $\mathbf{r}_{i\alpha}$  the position of site  $i\alpha$ , and  $N_0$

is the number of condensed particles. The bosonic operator  $c_{i\alpha}$  annihilates fluctuations on top of the condensate. By retaining only terms quadratic in the fluctuations, we obtain the Hamiltonian

$$\begin{aligned} \frac{H}{N} &= \frac{1}{2N} \boldsymbol{\psi}^\dagger H_B \boldsymbol{\psi} + E_c \\ H_B &= \begin{pmatrix} H_{\text{kin}} - \mu_{\text{eff}} & \Delta \\ \Delta^\dagger & H_{\text{kin}}^* - \mu_{\text{eff}} \end{pmatrix}, \\ \boldsymbol{\psi}^\dagger &= \left( c_{11}^\dagger, \dots, c_{N_c, N_b}^\dagger, c_{11}, \dots, c_{N_c, N_b} \right), \end{aligned} \quad (2)$$

where  $[\Delta]_{i\alpha, j\beta} = UNn_0\varphi_{i\alpha}^2\delta_{i\alpha, j\beta}$  and  $[\mu_{\text{eff}}]_{i\alpha, j\beta} = \mu - 2UNn_0|\varphi_{i\alpha}|^2\delta_{i\alpha, j\beta}$ . We define  $n_0 = N_0/N$ , where  $N = N_c N_b$  is the total number of sites,  $N_b$  the number of bands and  $N_c$  the number unit cells. The energy  $E_c$  relates to the ground state energy of the condensate [67].

The state  $|\varphi_0\rangle$  is determined by minimizing the mean-field energy

$$E_{\text{MF}} = n_0 \langle \varphi_0 | H_{\text{kin}} | \varphi_0 \rangle - n_0 \mu + N \frac{Un_0^2}{2} \sum_{i\alpha} |\varphi_{i\alpha}|^4 \quad (3)$$

while enforcing the normalization  $\langle \varphi_0 | \varphi_0 \rangle = 1$ . In a flat band,  $\langle \varphi_0 | H_{\text{kin}} | \varphi_0 \rangle = \varepsilon_0$  is a constant, and we simply need to minimize  $\sum_{i\alpha} |\varphi_{i\alpha}|^4$ . Whenever possible,  $|\varphi_0\rangle$  will therefore have uniform densities,  $|\varphi_{i\alpha}| = 1/\sqrt{N}$ . This work focuses on models where at least one such uniform-density state exists on the flat band.

The Hamiltonian (2) can be written in a diagonal form with  $\boldsymbol{\psi}^\dagger H_B \boldsymbol{\psi} = \boldsymbol{\gamma}^\dagger \boldsymbol{\varepsilon} \boldsymbol{\gamma}$ , where  $\boldsymbol{\gamma}^\dagger = (\gamma_{1+}^\dagger, \dots, \gamma_{N+}^\dagger, \gamma_{1-}, \dots, \gamma_{N-})$  contains Bogoliubov boson operators and  $\boldsymbol{\varepsilon}$  the corresponding energies. Because  $\gamma_{i\sigma}^\dagger, \gamma_{i\sigma}$  need to fulfill bosonic commutation relations, we carry out a paraunitary standardization of  $H_B$  (see Refs. [68–70] and supplementary material [67]). In practice,  $\boldsymbol{\gamma}^\dagger$  and  $\boldsymbol{\varepsilon}$  can be determined from the Jordan normal form of the non-Hermitian matrix  $\gamma_z H_B$ , with  $\gamma_z = \sigma_z \otimes \mathbb{1}_N$  [71]. In our case,  $\gamma_z H_B$  has real eigenvalues and a one-dimensional kernel spanned by  $(|\varphi_0\rangle, -|\varphi_0^*\rangle)^T$ . Additional vanishing eigenvalues would indicate that condensation is not possible in  $|\varphi_0\rangle$  alone, at least within traditional Bogoliubov theory.

Keeping this important point in mind, let us assume that there exists a pair of flat-band eigenstates  $|\varphi'_0\rangle = C|\varphi_0\rangle$  and  $|\varphi''_0\rangle = C^\dagger|\varphi_0\rangle$ , where  $C$  is a diagonal complex matrix,  $[C]_{i\alpha, i\alpha} = a_{i\alpha} e^{i\xi_{i\alpha}}$ , with  $a_{i\alpha}$  and  $\xi_{i\alpha}$  real numbers. Then  $\varphi'_{i\alpha} = e^{2i\xi_{i\alpha}} \varphi''_{i\alpha} = a_{i\alpha} e^{i\xi_{i\alpha}} \varphi_{i\alpha}$ . The key observation is that

$$\begin{aligned} & [(H_{\text{kin}} - \mu_{\text{eff}}) |\varphi'_0\rangle - \Delta |\varphi''_0\rangle]_{i\alpha} \\ &= \varepsilon_0 \varphi'_{i\alpha} - \mu_{\text{eff}} \varphi'_{i\alpha} - UNn_0 \varphi_{i\alpha}^2 (\varphi''_{i\alpha})^* \\ &= UN \left( 1 - \frac{N |\varphi'_{i\alpha}|^2}{a_{i\alpha}^2} e^{-2i\xi_{i\alpha}} e^{2i\xi_{i\alpha}} \right) \varphi'_{i\alpha} = 0. \end{aligned} \quad (4)$$

On the second line, we have used that  $|\varphi'_0\rangle$  is a flat-band eigenstate, i.e.  $H_{\text{kin}} |\varphi'_0\rangle = \varepsilon_0 |\varphi'_0\rangle$ . On the third line,

we have plugged in the effective chemical potential for a uniform-density flat-band condensate,  $\mu_{\text{eff}} = \varepsilon_0 - Un_0$  [67], and used the fact that  $|\varphi'_{i\alpha}|^2 = a_{i\alpha}^2/N$ . A similar reasoning shows that  $[(H_{\text{kin}}^* - \mu_{\text{eff}}) |\varphi''_0\rangle - \Delta^\dagger |\varphi'_0\rangle] = 0$ .

It follows that  $\gamma_z H_B (|\varphi'_0\rangle, -|\varphi''_0\rangle)^T = 0$ : the kernel of  $\gamma_z H_B$  contains at least both  $(|\varphi_0\rangle, -|\varphi_0^*\rangle)^T$  and  $(|\varphi'_0\rangle, -|\varphi''_0\rangle)^T$ . When  $C$  is not proportional to the identity matrix,  $|\varphi_0\rangle$ ,  $|\varphi'_0\rangle$  and  $|\varphi''_0\rangle$  are not simply related by a gauge transformation, and the kernel of  $\gamma_z H_B$  is at least two-dimensional. This goes against the assumption of condensation in a single mode.

On a flat band, for a stable condensate in  $|\varphi_0\rangle$ , excluding gauge transformations, there should therefore exist no pairs of flat-band states  $C|\varphi_0\rangle, C^\dagger|\varphi_0\rangle$  with  $C$  a diagonal matrix. In the particular case that there exists a state  $R|\varphi_0\rangle$ , where  $R$  is a real diagonal matrix not proportional to the identity, this single state is sufficient to destabilize condensation in  $|\varphi_0\rangle$ . It is important to note that  $C$  and  $R$  do not need to be unitary: the states destabilizing condensation do not need to minimize  $E_{\text{MF}}$ , emphasizing that flat-band condensation can be destabilized by geometric effects even when  $E_{\text{MF}}$  has a non-degenerate minimum.

### III. COMPACT LOCALIZED STATES AND FLAT-BAND CONDENSATION

To determine whether condensation is possible on a flat band, we first need to find the possible states  $|\varphi_0\rangle$ , and then to check whether other problematic states  $C|\varphi_0\rangle, C^\dagger|\varphi_0\rangle$  exist for each of these states. To this end, we expand the flat-band states in terms of CLSs and non-contractible loop states (NLS). CLSs are single-particle flat-band eigenstates localized by destructive interference that have a nonzero amplitude in a finite region of space, and vanish elsewhere (see Fig. 1a-b). Because of the translational symmetry of the lattice, we can associate a CLS  $|\nu_{i,n}\rangle$  with each unit cell  $i$ :

$$|\nu_{i,n}\rangle = \sum_{j\alpha} \nu_{\mathbf{R}_j\alpha, n} |(\mathbf{R}_i + \mathbf{R}_j)\alpha\rangle, \quad (5)$$

where  $j$  runs over unit cells,  $\mathbf{R}_i$  is the center of the  $i$ th unit cell, and  $\nu_{\mathbf{R}_j\alpha, n}$  are the amplitudes of the CLSs associated with  $\mathbf{R}_i = 0$  at site  $j\alpha$ . The index  $n$  runs over degenerate flat bands,  $n = 1 \dots N_{\text{fb}}$ , i.e. for  $N_{\text{fb}}$  degenerate bands, there are  $N_{\text{fb}}$  CLSs associated with each unit cell. CLSs can be constructed for any flat band of a tight-binding model with finite-range hopping processes [41].

While we can associate one CLS to each unit cell, they are not always linearly independent in systems with periodic boundary conditions [41, 42]. This occurs in so-called singular bands [40, 41], which can not be spanned by CLSs alone and require NLSs (see Fig. 1a-b) or other extended states. We refer to these additional states as  $|\tilde{\nu}_a\rangle = \sum_{i\alpha} \tilde{\nu}_{i\alpha, a} |\mathbf{R}_i\alpha\rangle$ , where  $a$  labels the states. The states  $|\nu_{i,n}\rangle$  and  $|\tilde{\nu}_a\rangle$  fully span the flat bands, and all

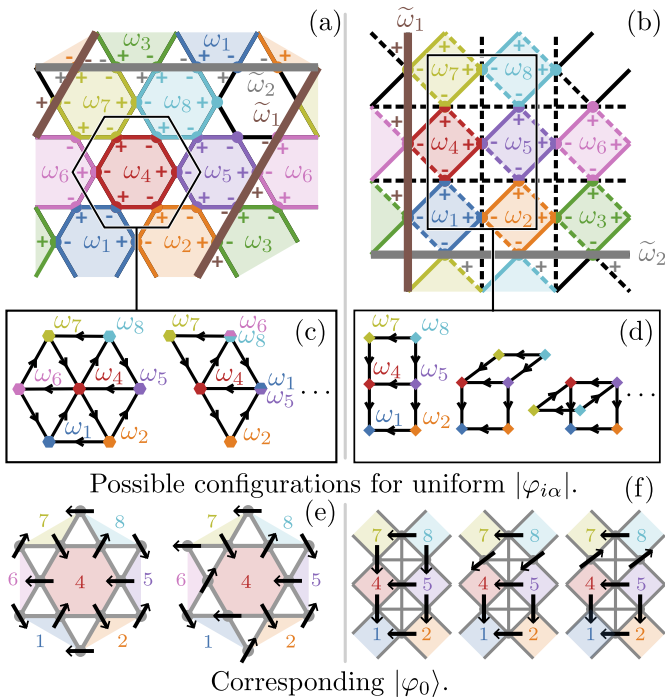


FIG. 1. CLSs (hexagons/squares of different colors) and NLSs (thick brown/gray lines) in (a) the kagome lattice and (b) the checkerboard lattice, in a system of  $3 \times 3$  unit cells with periodic boundary conditions. Full lines indicate a hopping amplitude  $t = 1$ , while dashed lines indicate  $t = -1$ . Considering the overlaps of CLSs at sites within the region bounded by a thin black line, and requiring uniform  $|\varphi_{i\alpha}|$ , we obtain a set of constraints  $|\omega_i - \omega_j| = 1/\sqrt{N}$  for neighboring  $\omega_i$  and  $\omega_j$ , fixing the distance between these points in the complex plane. (c-d) Examples of possible configurations of coefficients  $\omega_i$  in the complex plane in the (c) kagome and (d) checkerboard lattices. Each edge of the frameworks has length  $1/\sqrt{N}$ , and corresponds to  $\varphi_{i\alpha}$  at a given site. The resulting  $|\varphi_0\rangle$  are shown in (e-f).

eigenstates with  $H_{\text{kin}}|\psi\rangle = \varepsilon_0|\psi\rangle$  can be written as a linear combination

$$|\psi\rangle = \sum_{i,n} \omega_{i,n} |\nu_{i,n}\rangle + \sum_a \tilde{\omega}_a |\tilde{\nu}_a\rangle. \quad (6)$$

The choice of CLSs and NLSs is not unique, but any complete basis is valid for the following arguments [67].

As stated previously, we focus on systems where there exists at least one flat-band eigenstate with uniform  $|\varphi_{i\alpha}| = 1/\sqrt{N}$ , which is guaranteed to minimize  $E_{\text{MF}}$ . All such states fulfill the constraints

$$\left| \sum_{j,n} \nu_{(\mathbf{R}_i - \mathbf{R}_j)\alpha,n} \omega_{j,n} + \sum_a \tilde{\nu}_{i\alpha,a} \tilde{\omega}_a \right| = \frac{1}{\sqrt{N}}, \quad (7)$$

obtained by requiring that for each  $i\alpha$ ,  $|\psi_{i\alpha}| = 1/\sqrt{N}$  in Eq. (6). The problem of finding all states minimizing  $E_{\text{MF}}$  is equivalent to the geometric problem of finding the possible positions of  $\omega_{j,n}$  and  $\tilde{\omega}_a$  in the complex plane while fulfilling all the constraints (7).

As two simple examples, let us consider the kagome and checkerboard lattices (Fig. 1). These lattices both feature a lowest flat band with a singular band touching [67]. We first consider sites where two CLSs overlap with opposite signs and NLSs are not involved (Fig. 1a-b). The constraints (7) corresponding to these sites acquire the form  $|\omega_i - \omega_j| = 1/\sqrt{N}$ , where we have omitted the index  $n$  since we consider a single flat band. The distance in the complex plane between  $\omega_i$  and  $\omega_j$  corresponding to neighboring CLSs is therefore  $1/\sqrt{N}$ . In the kagome lattice, this is fulfilled only when the coefficients  $\omega_i$  are the vertices of a triangular framework (see Fig. 1c), while on the checkerboard lattice, the coefficients lie on a square framework (see Fig. 1d). Each edge of these frameworks corresponds to  $\varphi_{i\alpha}$  at one site (see Fig. 1e-f). When also sites involving NLSs are taken into account, the configurations shown in Fig. 1(c-d) become compatible with periodic boundary conditions [67].

Because only the distances between neighboring coefficients are fixed, there are many configurations of  $\omega_i$  fulfilling all constraints (7) in both lattices. Some operations have no physical impact: translating the whole framework does not change the directions of any of the edges, and thus does not change the corresponding wavefunction, while an overall rotation is a gauge transformation. However, other transformations give a new uniform-density flat-band eigenstate. In the kagome lattice, while the triangles can not be deformed without changing edge lengths (or equivalently, without changing  $|\varphi_{i\alpha}|$ ), two triangles sharing an edge can point in opposite or identical directions. In other words, "folding" or "unfolding" along edges of the triangular framework yields new configurations minimizing  $E_{\text{MF}}$  (see Fig. 1(c)). In the checkerboard lattice, angles between edges of the framework can be changed continuously without affecting edge lengths (see Fig. 1(d)), reflecting that states minimizing  $E_{\text{MF}}$  are connected by continuous transformations which leave  $E_{\text{MF}}$  unchanged.

In the kagome and checkerboard lattices, Eq. (7) simply constrains distances between coefficients  $\omega_i$ . In more complicated cases, Eq. (7) constrains the distance between linear combinations of several  $\omega_i$ . Flat band states can then be represented as frameworks where each edge corresponds to  $b_{i\alpha}\varphi_{i\alpha}$ , with  $b_{i\alpha}$  a scalar, and each vertex is a linear combination of coefficients  $\omega_i$ .

This approach allows us to geometrically determine all flat-band states which minimize  $E_{\text{MF}}$ . To verify that condensation is possible, we now need to ensure for these  $|\varphi_0\rangle$  that there exist no problematic states  $C|\varphi_0\rangle, C^\dagger|\varphi_0\rangle$ . Since all flat-band states are spanned by CLSs and NLSs, they can be represented by frameworks with the same underlying graph, but potentially different edge lengths, as the ones representing the states minimizing  $E_{\text{MF}}$ . Every complex diagonal matrix can be rewritten as  $C = RU$ , where  $R$  is a real diagonal matrix and  $U$  is a unitary diagonal matrix. Multiplication by a real diagonal matrix  $R$  corresponds to changing the lengths of edges while keeping

them parallel to their initial direction. Multiplication by a diagonal unitary matrix  $U$  corresponds to rotating each edge by an angle  $\xi_{i\alpha}$ . Condensation is unstable in a given  $|\varphi_0\rangle$  if, excluding overall rotations and uniform scaling, it is possible to construct 1) a framework with all edges parallel to those of the framework representing  $|\varphi_0\rangle$  or 2) two frameworks with edges rotated by  $+\xi_{i\alpha}$ ,  $-\xi_{i\alpha}$  respectively compared to their original orientation, and both having identical edge lengths.

In the checkerboard lattice, condensation is impossible in any uniform-density  $|\varphi_0\rangle$ : we can flip the direction of a subset of edges without changing the orientation of others, yielding a different framework with all edges parallel to their original direction (see Fig. 1(d)). In the kagome lattice, each  $|\varphi_0\rangle$  is represented by a framework consisting of only triangles with nonzero area, which we refer to as a triangulated framework. For such frameworks, the problematic frameworks mentioned above can not be constructed, and condensation can occur [67]. Other lattices where all possible  $|\varphi_0\rangle$  correspond to triangulated frameworks include for instance the sawtooth ladder [67].

In complicated models, it might be difficult to directly visualize all  $|\varphi_0\rangle$  as frameworks. As outline in the supplementary material, it is also possible to directly verify from a basis of CLSs and NLSs whether states  $C|\varphi_0\rangle$ ,  $C^\dagger|\varphi_0\rangle$  exist for a given  $|\varphi_0\rangle$ , without explicitly considering frameworks [67]. However, this requires the prior determination of  $|\varphi_0\rangle$ .

#### IV. TASAKI LATTICE WITH STABLE FLAT-BAND CONDENSATION

Based on our observations, we can construct CLSs that are compatible with condensation: we simply need to ensure that they overlap in such a way that uniform-density flat-band eigenstates are represented by triangulated frameworks. An example, as well as a possible configuration of  $\omega_i$  that minimizes  $E_{\text{MF}}$ , are shown in Fig. 2a-b. We work on a Tasaki lattice [72], with the tight-binding parameters shown in Fig. 2c (note that tight-binding parameters for a given CLS are not unique). We introduce a tuning parameter  $a$  which controls the possible phases of  $\omega_i$  when  $E_{\text{MF}}$  is minimized: in adjacent unit cells  $i$  and  $j$ ,  $\omega_i = \omega_j e^{\pm i\theta}$ , where  $\theta = 2 \arcsin(a/2)$ . This implies that the Bloch states at  $\mathbf{k} = 2 \arcsin(a/2)(\sigma, \sigma')$ , with  $\sigma, \sigma' = \pm 1$  have uniform densities.

When using periodic boundary conditions, uniform-density flat-band states are commensurate with the system size only for a few values of  $a$  at numerically accessible system sizes. We therefore use open boundary conditions. In order to retain the perfect flatness of the band and the uniformity of  $|\varphi_0\rangle$ , the tight-binding parameters at the boundaries are adjusted (detailed parameters are given in the supplementary material [67]).

To determine which state is the most favorable for con-

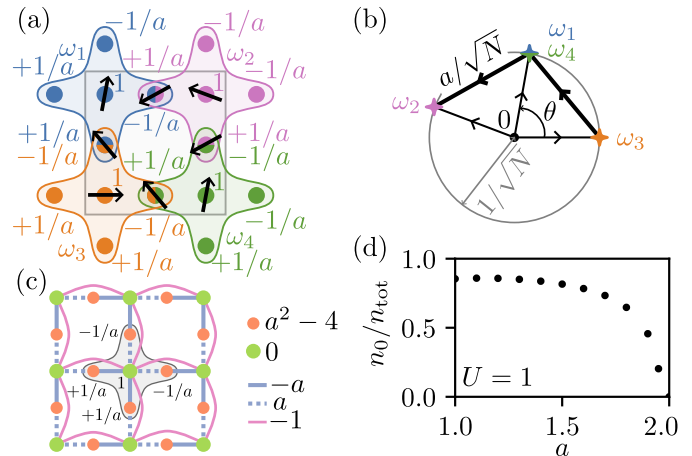


FIG. 2. (a) CLSs used as a starting point for the construction of a model with stable flat-band condensation. Each CLS is centered on a site where there are no overlaps, which constrains  $|\omega_i| = 1/\sqrt{N}$  to achieve uniform densities. The amplitude of the CLS at other sites is  $\pm 1/a$ , and the overlaps with adjacent CLSs enforce  $|\omega_i - \omega_j| = a/\sqrt{N}$ . Together, these constraints then require that  $0, \omega_i$  and  $\omega_j$  form an isosceles triangle. (b) Possible configuration for the coefficients  $\omega_i$ , under the constraints related to the sites in the gray square in (a). The thin black edges have a length of  $1/\sqrt{N}$ , and correspond to  $\varphi_{i\alpha}$  at the central site of a CLS. The thick black lines have a length of  $a/\sqrt{N}$ , and give  $a\varphi_{i\alpha}$  for the other sites. The  $\varphi_{i\alpha}$  corresponding to this configuration are indicated by arrows in (a). (c) Tight-binding model for the Tasaki lattice considered here. (d) Condensate fraction  $n_0/n_{\text{tot}}$  assuming condensation in the uniform-density state with the lowest ZPE. We set  $n_{\text{tot}} = 1$ .

densation, we compute the zero-point energy (ZPE) of the Bogoliubov phonons corresponding to randomly sampled uniform-density  $|\varphi_0\rangle$ . The sampling is performed by taking advantage of a correspondence between the possible  $|\varphi_0\rangle$  and three-colorings of a square lattice [67]. The three-coloring sampling was performed using the Wang-Swendsen-Kotecký (WSK) algorithm [73, 74]. Although this algorithm is not always ergodic [75–77], the ergodicity is guaranteed on bipartite lattices [78], including the square lattice.

The state  $|\varphi_0\rangle$  with the lowest ZPE, which is the most favorable for condensation, is a superposition of the  $\mathbf{k} = (0, 0)$  and  $\mathbf{k} = (\pi, \pi)$  Bloch states, while the least favorable  $|\varphi_0\rangle$  are the Bloch states at  $\mathbf{k}_c = 2 \arcsin(a/2)(\sigma, \sigma')$  (see supplementary material [67] for details). Assuming condensation in the most favorable state,  $n_0$  is nonzero, signaling condensation is possible, except in the limit  $a \rightarrow 2$  (see Fig. 2d).

At  $a = 2$ , the area of the triangles in Fig. 2b vanishes, and  $E_{\text{MF}}$  is minimized by only the  $(\pi, \pi)$  Bloch state. However, even though there is no degeneracy at the mean-field level, condensation becomes unstable because of the existence of problematic non-uniform flat-band eigenstates [67]. This highlights that also states that do not minimize  $E_{\text{MF}}$  can destabilize the condensate due

to quantum geometric effects.

## V. RELATIONSHIP TO THE CONDENSATE QUANTUM DISTANCE

Our method has some similarity to previous quantum geometric approaches, since it predicts the possibility of a stable condensate from the properties of the non-interacting model. Quantum geometry and the properties of CLSs and NLSs can give complementary information for instance in the context of singular bands: the necessity of NLSs relates directly to the singularity of the band touching and the existence of boundary states in systems with open boundary conditions, while the quantum distance gives information on the strength of the singularity [79–81]. Similarly, our method complements previous research relating the quantum distance to the excitation fraction.

When condensation is assumed to occur in a Bloch state  $|n_{\mathbf{k}_c}\rangle$  corresponding to a momentum  $\mathbf{k}_c$  on a single non-degenerate flat band, it was shown in Refs. [32, 34] that the excitation fraction is related to the so-called condensate quantum distance  $D(\mathbf{q})$  by

$$\begin{aligned} \lim_{U \rightarrow 0} n_{\text{ex}} &= \frac{1}{N_c} \sum_{\mathbf{q} \neq 0} \frac{1 - D(\mathbf{q})}{2D(\mathbf{q})}, \\ D(\mathbf{q}) &= \sqrt{1 - |\delta(\mathbf{q})|^2}, \\ \delta(\mathbf{q}) &= N_b \sum_{\alpha} \langle n_{\mathbf{k}_c + \mathbf{q}} | \alpha \rangle \langle n_{\mathbf{k}_c - \mathbf{q}} | \alpha \rangle \langle \alpha | n_{\mathbf{k}_c} \rangle^2, \end{aligned} \quad (8)$$

where  $|n_{\mathbf{k}}\rangle$  is the periodic part of the Bloch function on the flat band and  $|\langle \alpha | n_{\mathbf{k}_c} \rangle|^2 = 1/N_b$ , i.e.  $|\varphi_0\rangle$  is again assumed to have uniform densities. In real space,  $|n_{\mathbf{k}}\rangle$  corresponds to a flat-band eigenstate such that  $\varphi_{i\alpha} = \langle \alpha | n_{\mathbf{k}} \rangle e^{i\mathbf{k} \cdot \mathbf{r}_{i\alpha}} / \sqrt{N_c}$ . The condensate quantum distance reduces to the usual quantum distance  $d(\mathbf{q}) = \sqrt{1 - |\langle n_{\mathbf{k}_c + \mathbf{q}} | n_{\mathbf{k}_c - \mathbf{q}} \rangle|^2}$  when all Bloch states are real.

In this work, we determine whether states  $|\varphi'_0\rangle = C|\varphi_0\rangle$ ,  $|\varphi''_0\rangle = C^\dagger|\varphi_0\rangle$  exist on the flat band for any given  $|\varphi_0\rangle$ . When  $|\varphi_0\rangle$  is a Bloch state,  $\varphi'_{i\alpha} = a_{i\alpha} e^{i\mathbf{k}_c \cdot \mathbf{r}_{i\alpha}} e^{i\xi_{i\alpha}} / \sqrt{N}$ ,  $\varphi''_{i\alpha} = a_{i\alpha} e^{i\mathbf{k}_c \cdot \mathbf{r}_{i\alpha}} e^{-i\xi_{i\alpha}} / \sqrt{N}$ . These two states will also be Bloch states when  $a_{i\alpha} = a_\alpha$  is independent of the unit cell, and  $\xi_{i\alpha} = \xi_\alpha + \mathbf{q} \cdot \mathbf{r}_{i\alpha}$  for some momentum  $\mathbf{q}$ . In other words, if we require that  $|\varphi_0\rangle$ ,  $|\varphi'_0\rangle$  and  $|\varphi''_0\rangle$  are Bloch states,  $|\varphi'_0\rangle$  and  $|\varphi''_0\rangle$  will correspond to Bloch states  $|n_{\mathbf{k}_c + \mathbf{q}}\rangle$  and  $|n_{\mathbf{k}_c - \mathbf{q}}\rangle$  with periodic parts  $|n_{\mathbf{k}_c + \mathbf{q}}\rangle = \tilde{C}|n_{\mathbf{k}_c}\rangle$ ,  $|n_{\mathbf{k}_c - \mathbf{q}}\rangle = \tilde{C}^\dagger|n_{\mathbf{k}_c}\rangle$ , where  $\tilde{C}$  is a diagonal matrix. If such states indeed exist,

$$\delta(\mathbf{q}) = \frac{1}{N_b} \sum_{\alpha} \tilde{C}_{\alpha\alpha}^2 = 1, \quad (9)$$

where we have used that  $\langle n_{\mathbf{k}_c + \mathbf{q}} | n_{\mathbf{k}_c + \mathbf{q}} \rangle = (1/N_b) \sum_{\alpha} \tilde{C}_{\alpha\alpha}^2 = 1$ . It follows that the condensate quantum distance vanishes at  $\mathbf{q}$ , and  $n_{\text{ex}}$  diverges. When restricting the analysis to Bloch states, the real-space

approach used here thus relies on a necessary condition for the quantum distance to be nonzero at all  $\mathbf{q} \neq 0$ . This approach is however more general, since it also accounts for states that might destabilize the condensate but are not Bloch states.

## VI. DISCUSSION

We have shown how the possibility of stable condensation on a flat band is influenced by how CLSs overlap, which determines constraints for states minimizing the mean-field energy. These states can be visualized as frameworks, and a triangulated framework is promising for condensation. Based on this observation, it is possible to construct flat-band models with potential for a stable Bose-Einstein condensate by using an advantageous basis of CLSs as a starting point. This method could be used for instance to build models that can be implemented experimentally, or that have desired properties such as topologically nontrivial flat bands.

This work provides further insight into bosonic flat-band systems, complementing previous research relating the stability of flat-band condensates and superfluids to quantum geometric quantities [32–36]. It re-emphasizes the important impact of the geometry of eigenstates, sometimes including those without translational invariance, on flat-band properties.

This method could also give insight into phases occurring at temperatures where Bose-Einstein condensation does not yet occur. Previously, a trion phase has been predicted above the temperature for Bose-Einstein condensation in the kagome lattice [30]. This is related to the structure of the flat-band eigenstates minimizing the mean-field energy: the phases of uniform-density state are constrained to multiples of  $2\pi/3$ . In this work, we constructed an example of a flat band model where the possible phases are still constrained, but can take more than three distinct values. Similar constraints on possible phases are likely to occur in many flat bands with a stable condensate, since stability has a relation to triangulated frameworks, where edge direction can not be continuously modified. Similarly to the kagome lattice, such constraints could manifest for instance in time-of-flight measurements [30, 82].

*Acknowledgments* — The author thanks Sebastian D. Huber and Friederike Bartels for fruitful discussion, and Matteo Dürrnagel for helpful comments. The author gratefully acknowledges support by an ETH Zürich Postdoctoral Fellowship.

---

\* [khuhtinen@phys.ethz.ch](mailto:khuhtinen@phys.ethz.ch)

[1] P. Törmä, S. Peotta, and B. A. Bernevig, Superconductivity, superfluidity and quantum geometry in twisted multilayer systems, *Nature Reviews Physics* **4**, 528 (2022).

- [2] L. Zheng, L. Feng, and W. Yong-Shi, Exotic electronic states in the world of flat bands: From theory to material, *Chinese Physics B* **23**, 077308 (2014).
- [3] H. Tasaki, From Nagaoka's ferromagnetism to flat-band ferromagnetism and beyond: An introduction to ferromagnetism in the Hubbard model, *Progress of Theoretical Physics* **99**, 489 (1998).
- [4] J. P. Provost and G. Vallee, Riemannian structure on manifolds of quantum states, *Communications in Mathematical Physics* **76**, 289 (1980).
- [5] S. Peotta and P. Törmä, Superfluidity in topologically non-trivial flat bands, *Nature Communications* **6**, 8944 (2015).
- [6] E. Rossi, Quantum metric and correlated states in two-dimensional systems, *Current Opinion in Solid State and Materials Science* **25**, 100952 (2021).
- [7] S. Peotta, K.-E. Huhtinen, and P. Törmä, Quantum geometry in superfluidity and superconductivity, *arXiv e-prints*, arXiv:2308.08248 (2023), arXiv:2308.08248 [cond-mat.quant-gas].
- [8] R. Resta, The insulating state of matter: a geometrical theory, *The European Physical Journal B* **79**, 121 (2011).
- [9] J. Ahn and N. Nagaosa, Superconductivity-induced spectral weight transfer due to quantum geometry, *Physical Review B* **104**, L100501 (2021).
- [10] G. E. Topp, C. J. Eckhardt, D. M. Kennes, M. A. Sentef, and P. Törmä, Light-matter coupling and quantum geometry in moiré materials, *Physical Review B* **104**, 064306 (2021).
- [11] N. Verma, T. Hazra, and M. Randeria, Optical spectral weight, phase stiffness, and  $T_c$  bounds for trivial and topological flat band superconductors, *Proceedings of the National Academy of Sciences* **118**, e2106744118 (2021).
- [12] J.-X. Hu, S. A. Chen, and K. T. Law, Geometric and conventional contributions of superconducting diode effect: Application to flat-band systems, *Physical Review B* **111**, 174513 (2025).
- [13] H. Tanaka, H. Watanabe, and Y. Yanase, Nonlinear optical response in superconductors in magnetic field: Quantum geometry and topological superconductivity, *Physical Review B* **110**, 014520 (2024).
- [14] I. Komissarov, T. Holder, and R. Queiroz, The quantum geometric origin of capacitance in insulators, *Nature Communications* **15**, 4621 (2024).
- [15] N. Verma and R. Queiroz, Framework to measure quantum metric from step response, *Physical Review Letters* **134**, 106403 (2025).
- [16] S. Taie, H. Ozawa, T. Ichinose, T. Nishio, S. Nakajima, and Y. Takahashi, Coherent driving and freezing of bosonic matter wave in an optical Lieb lattice, *Science Advances* **1**, e1500854 (2015).
- [17] S. Mukherjee, A. Spracklen, D. Choudhury, N. Goldman, P. Öhberg, E. Andersson, and R. R. Thomson, Observation of a localized flat-band state in a photonic Lieb lattice, *Physical Review Letters* **114**, 245504 (2015).
- [18] R. A. Vicencio, C. Cantillano, L. Morales-Inostroza, B. Real, C. Mejía-Cortés, S. Weimann, A. Szameit, and M. I. Molina, Observation of localized states in Lieb photonic lattices, *Physical Review Letters* **114**, 245503 (2015).
- [19] S. Kajiwara, Y. Urade, Y. Nakata, T. Nakanishi, and M. Kitano, Observation of a nonradiative flat band for spoof surface plasmons in a metallic Lieb lattice, *Physical Review B* **93**, 075126 (2016).
- [20] T. H. Harder, O. A. Egorov, J. Beierlein, P. Gagel, J. Michl, M. Emmerling, C. Schneider, U. Peschel, S. Höfling, and S. Klemmt, Exciton-polaritons in flatland: Controlling flatband properties in a Lieb lattice, *Physical Review B* **102**, 121302 (2020).
- [21] F. Baboux, L. Ge, T. Jacqmin, M. Biondi, E. Galopin, A. Lemaître, L. Le Gratiet, I. Sagnes, S. Schmidt, H. E. Türeci, A. Amo, and J. Bloch, Bosonic condensation and disorder-induced localization in a flat band, *Physical Review Letters* **116**, 066402 (2016).
- [22] C. E. Whittaker, E. Cancellieri, P. M. Walker, D. R. Gulevich, H. Schomerus, D. Vaitiekus, B. Royall, D. M. Whittaker, E. Clarke, I. V. Iorsh, I. A. Shelykh, M. S. Skolnick, and D. N. Krizhanovskii, Exciton polaritons in a two-dimensional Lieb lattice with spin-orbit coupling, *Physical Review Letters* **120**, 097401 (2018).
- [23] F. Scafirimuto, D. Urbonas, M. A. Becker, U. Scherf, R. F. Mahrt, and T. Stöferle, Tunable exciton-polariton condensation in a two-dimensional Lieb lattice at room temperature, *Communications Physics* **4**, 39 (2021).
- [24] T. H. Harder, O. A. Egorov, C. Krause, J. Beierlein, P. Gagel, M. Emmerling, C. Schneider, U. Peschel, S. Höfling, and S. Klemmt, Kagome flatbands for coherent exciton-polariton lasing, *ACS Photonics* **8**, 3193 (2021).
- [25] F. Jin, J. Ren, S. Zanotti, P. Cui, H. Zheng, J. Liang, J. Ni, Z. Wang, F. Shi, C.-W. Qiu, G. Chang, T. C. H. Liew, and R. Su, Exciton polariton condensation in a perovskite moiré flat band at room temperature, *Science Advances* **11**, eadx2361 (2025).
- [26] J. Wei, X. Zhai, Q. Ai, C. Xing, X. Yang, Y. Cai, T. Wang, X. He, D. Wang, S. An, T. Liu, H. Dai, L. Feng, and T. Gao, Condensation of exciton polaritons in a flatband of a deformed triangle lattice at room temperature, *Applied Physics Letters* **126**, 152110 (2025).
- [27] H. Li, Q. Liang, Z. Dong, H. Wang, W. Yi, J.-S. Pan, and B. Yan, Engineering topological chiral transport in a flat-band lattice of ultracold atoms, *Light: Science & Applications* **14**, 326 (2025).
- [28] Z. Meng, L. Wang, W. Han, F. Liu, K. Wen, C. Gao, P. Wang, C. Chin, and J. Zhang, Atomic Bose-Einstein condensate in twisted-bilayer optical lattices, *Nature* **615**, 231 (2023).
- [29] S. D. Huber and E. Altman, Bose condensation in flat bands, *Physical Review B* **82**, 184502 (2010).
- [30] Y.-Z. You, Z. Chen, X.-Q. Sun, and H. Zhai, Superfluidity of bosons in kagome lattices with frustration, *Physical Review Letters* **109**, 265302 (2012).
- [31] Z. Jalali-mola, T. Grass, V. Kasper, M. Lewenstein, and U. Bhattacharya, Topological Bogoliubov quasiparticles from Bose-Einstein condensate in a flat band system, *Physical Review Letters* **131**, 226601 (2023).
- [32] A. Julku, G. M. Bruun, and P. Törmä, Quantum geometry and flat band Bose-Einstein condensation, *Physical Review Letters* **127**, 170404 (2021).
- [33] A. Julku, G. M. Bruun, and P. Törmä, Excitations of a Bose-Einstein condensate and the quantum geometry of a flat band, *Physical Review B* **104**, 144507 (2021).
- [34] A. Julku, G. Salerno, and P. Törmä, Superfluidity of flat band Bose-Einstein condensates revisited, *Low Temperature Physics* **49**, 701 (2023).
- [35] I. Lukin, A. Sotnikov, and A. Kruchkov, Unconventional superfluidity and quantum geometry of topological bosons, *arXiv e-prints*, arXiv:2307.08748 (2023), arXiv:2307.08748 [cond-mat.quant-gas].
- [36] M. Iskin, Quantum-geometric contribution to the Bogoli-

- ubov modes in a two-band bose-einstein condensate, *Physical Review A* **107**, 023313 (2023).
- [37] K.-E. Huhtinen, M. Dürnagel, V. Peri, and S. D. Huber, Interplay of local and global quantum geometry in the stability of flat-band superfluids (2026).
- [38] B. Sutherland, Localization of electronic wave functions due to local topology, *Physical Review B* **34**, 5208 (1986).
- [39] H. Aoki, M. Ando, and H. Matsumura, Hofstadter butterflies for flat bands, *Physical Review B* **54**, R17296 (1996).
- [40] J.-W. Rhim and B.-J. Yang, Singular flat bands, *Advances in Physics: X* **6**, 1901606 (2021).
- [41] J.-W. Rhim and B.-J. Yang, Classification of flat bands according to the band-crossing singularity of bloch wave functions, *Physical Review B* **99**, 045107 (2019).
- [42] D. L. Bergman, C. Wu, and L. Balents, Band touching from real-space topology in frustrated hopping models, *Physical Review B* **78**, 125104 (2008).
- [43] Y. Hwang, J.-W. Rhim, and B.-J. Yang, Flat bands with band crossings enforced by symmetry representation, *Physical Review B* **104**, L081104 (2021).
- [44] D. Leykam, A. Andreanov, and S. Flach, Artificial flat band systems: from lattice models to experiments, *Advances in Physics: X* **3**, 1473052 (2018).
- [45] L. Tang, D. Song, S. Xia, S. Xia, J. Ma, W. Yan, Y. Hu, J. Xu, D. Leykam, and Z. Chen, Photonic flat-band lattices and unconventional light localization, *Nanophotonics* **9**, 1161 (2020).
- [46] S. Mukherjee and R. R. Thomson, Observation of localized flat-band modes in a quasi-one-dimensional photonic rhombic lattice, *Optics Letters* **40**, 5443 (2015).
- [47] S. Xia, Y. Hu, D. Song, Y. Zong, L. Tang, and Z. Chen, Demonstration of flat-band image transmission in optically induced Lieb photonic lattices, *Optics Letters* **41**, 1435 (2016).
- [48] Y. Zong, S. Xia, L. Tang, D. Song, Y. Hu, Y. Pei, J. Su, Y. Li, and Z. Chen, Observation of localized flat-band states in kagome photonic lattices, *Optics Express* **24**, 8877 (2016).
- [49] E. Travkin, F. Diebel, and C. Denz, Compact flat band states in optically induced flatland photonic lattices, *Applied Physics Letters* **111**, 011104 (2017).
- [50] H.-M. Lin, Y.-H. Lu, Y.-J. Chang, Y.-Y. Yang, and X.-M. Jin, Direct observation of a localized flat-band state in a mapped moiré Hubbard photonic lattice, *Physical Review Applied* **18**, 054012 (2022).
- [51] Y.-X. Shen, Y.-G. Peng, P.-C. Cao, J. Li, and X.-F. Zhu, Observing localization and delocalization of the flat-band states in an acoustic cubic lattice, *Physical Review B* **105**, 104102 (2022).
- [52] H. Hanafi, P. Menz, A. McWilliam, J. Imbrock, and C. Denz, Localized dynamics arising from multiple flat bands in a decorated photonic Lieb lattice, *APL Photonics* **7**, 111301 (2022).
- [53] L. Song, S. Gao, J. Ma, L. Tang, D. Song, Y. Li, and Z. Chen, Multiple flatbands and localized states in photonic super-kagome lattices, *Optics Letters* **48**, 5947 (2023).
- [54] C. Chase-Mayoral, L. Q. English, N. Lape, Y. Kim, S. Lee, A. Andreanov, S. Flach, and P. G. Kevrekidis, Compact localized states in electric circuit flat-band lattices, *Physical Review B* **109**, 075430 (2024).
- [55] E. Riva, F. Bellinzoni, and F. Braghin, Creating compact localized modes for robust sound transport via singular flat band engineering, *Communications Physics* **8**, 255 (2025).
- [56] H. Song, R. Zhang, and V. Van, Observation of compact localized states in synthetic Floquet-Lieb topological photonic lattices, *Communications Physics* **8**, 219 (2025).
- [57] C. Danieli, A. Andreanov, D. Leykam, and S. Flach, Flat band fine-tuning and its photonic applications, *Nanophotonics* **13**, 3925 (2024).
- [58] C. Danieli and S. Flach, *Progress on artificial flat band systems: classifying, perturbing, applying* (2026), arXiv:2603.04248 [cond-mat.mes-hall].
- [59] W. Maimaiti, A. Andreanov, H. C. Park, O. Gendelman, and S. Flach, Compact localized states and flat-band generators in one dimension, *Physical Review B* **95**, 115135 (2017).
- [60] W. Maimaiti, S. Flach, and A. Andreanov, Universal  $d = 1$  flat band generator from compact localized states, *Physical Review B* **99**, 125129 (2019).
- [61] W. Maimaiti, A. Andreanov, and S. Flach, Flat-band generator in two dimensions, *Physical Review B* **103**, 165116 (2021).
- [62] W. Maimaiti and A. Andreanov, Non-hermitian flat-band generator in one dimension, *Physical Review B* **104**, 035115 (2021).
- [63] Y. Hwang, J.-W. Rhim, and B.-J. Yang, General construction of flat bands with and without band crossings based on wave function singularity, *Physical Review B* **104**, 085144 (2021).
- [64] A. Graf and F. Piéchon, Designing flat-band tight-binding models with tunable multifold band touching points, *Physical Review B* **104**, 195128 (2021).
- [65] H. Kim, C.-g. Oh, and J.-W. Rhim, General construction scheme for geometrically nontrivial flat band models, *Communications Physics* **6**, 305 (2023).
- [66] B. Liu, S. Liu, Y. Zhang, C. He, J. Yang, and H. Xiang, Designing flat-band materials through compact localized state clusters, *Physical Review B* **112**, L241111 (2025).
- [67] See supplementary material for the band structures of the considered models, details on Bogoliubov theory, discussion of the role of the non-contractible loop states, details on how triangulated frameworks relate to stability, verification of the stability of condensation without explicitly considering frameworks representing wavefunctions, discussion of the basis-independence of the stability, and details on the sawtooth and Tasaki model.
- [68] J. H. P. Colpa, Diagonalization of the quadratic boson hamiltonian, *Physica A: Statistical Mechanics and its Applications* **93**, 327 (1978).
- [69] J. H. P. Colpa, Diagonalization of the quadratic boson hamiltonian with zero modes: I. Mathematical, *Physica A: Statistical Mechanics and its Applications* **134**, 377 (1986).
- [70] J. H. P. Colpa, Diagonalization of the quadratic boson hamiltonian with zero modes: II. Physical, *Physica A: Statistical Mechanics and its Applications* **134**, 417 (1986).
- [71] Q.-R. Xu, V. P. Flynn, A. Alase, E. Cobanera, L. Viola, and G. Ortiz, Squaring the fermion: The threefold way and the fate of zero modes, *Physical Review B* **102**, 125127 (2020).
- [72] H. Tasaki, Ferromagnetism in the Hubbard models with degenerate single-electron ground states, *Phys. Rev. Lett.* **69**, 1608 (1992).
- [73] J.-S. Wang, R. H. Swendsen, and R. Kotecký, Antiferromagnetic Potts models, *Physical Review Letters* **63**, 109 (1989).
- [74] J.-S. Wang, R. H. Swendsen, and R. Kotecký, Three-state antiferromagnetic Potts models: A Monte Carlo study,

- Physical Review B* **42**, 2465 (1990).
- [75] M. Lubin and A. D. Sokal, Comment on “Antiferromagnetic Potts models”, *Physical Review Letters* **71**, 1778 (1993).
  - [76] B. Mohar and J. Salas, A new Kempe invariant and the (non)-ergodicity of the Wang–Swendsen–Kotecký algorithm, *Journal of Physics A: Mathematical and Theoretical* **42**, 225204 (2009).
  - [77] B. Mohar and J. Salas, On the non-ergodicity of the Swendsen–Wang–Kotecký algorithm on the kagomé lattice, *Journal of Statistical Mechanics: Theory and Experiment* **2010**, P05016 (2010).
  - [78] J. Salas and A. D. Sokal, Ergodicity of the Wang–Swendsen–Kotecký algorithm on several classes of lattices on the torus, *Journal of Physics A: Mathematical and Theoretical* **55**, 415004 (2022).
  - [79] J.-W. Rhim, K. Kim, and B.-J. Yang, Quantum distance and anomalous Landau levels of flat bands, *Nature* **584**, 59 (2020).
  - [80] C.-g. Oh, D. Cho, S. Y. Park, and J.-W. Rhim, Bulk-interface correspondence from quantum distance in flat band systems, *Communications Physics* **5**, 320 (2022).
  - [81] A. Filusch and H. Fehske, Singular flat bands in the modified Haldane-dice model, *Physica B: Condensed Matter* **659**, 414848 (2023).
  - [82] L. Donini, *Bose-Hubbard physics in the kagome and triangular optical lattices at negative absolute temperature*, Ph.D. thesis, Cavendish Laboratory, University of Cambridge (2024).

## Supplemental material: Stability of flat-band Bose-Einstein condensation from the geometry of compact localized states

Kukka-Emilia Huhtinen

*Institute for Theoretical Physics, ETH Zurich, 8093 Zürich, Switzerland*

### I. BAND STRUCTURES OF CONSIDERED LATTICE MODELS

The band structure is obtained by Fourier transforming  $H_{\text{kin}}$  in a system with periodic boundary conditions and diagonalizing the resulting matrix  $[H_{\mathbf{k}}]_{\alpha\beta} = \sum_j t_{0\alpha,j\beta} e^{i\mathbf{k}\cdot\mathbf{R}_j}$ , where  $t_{i\alpha,j\beta}$  is the hopping amplitude between sites  $i\alpha$  and  $j\beta$ , and  $\mathbf{R}_j$  is the center of the  $j$ :th unit cell. In the kagome lattice, the Fourier transformation is given by

$$H_{\mathbf{k}}^{\text{kagome}} = \begin{pmatrix} 0 & 1 + e^{ik_1} & 1 + e^{ik_3} \\ 1 + e^{-ik_y} & 0 & 1 + e^{-ik_2} \\ 1 + e^{-ik_3} & 1 + e^{ik_2} & 0 \end{pmatrix}, \quad (\text{S1})$$

where  $k_1 = k_x$ ,  $k_2 = k_x/2 + \sqrt{3}k_y/2$ ,  $k_3 = k_x/2 - \sqrt{3}k_y/2$ , giving the band structure shown in Fig. S1(a). This model features a lowest flat band with a singular band touching at  $\Gamma$ .

The Fourier-transformed kinetic Hamiltonian for the checkerboard model considered in the main text is

$$H_{\mathbf{k}}^{\text{checkerboard}} = \begin{pmatrix} -2 \cos(k_x) & 1 + e^{-i(k_x - k_y)} - e^{ik_y} - e^{-ik_x} \\ 1 + e^{i(k_x - k_y)} - e^{-ik_y} - e^{ik_x} & -2 \cos(k_y) \end{pmatrix} \quad (\text{S2})$$

Like the kagome lattice, this lattice features a lowest flat band with a singular band touching at  $\Gamma$  (see Fig. S1(b)), but in contrast to the kagome lattice, the flat band can not host a stable condensate.

For the modified Tasaki lattice,

$$H_{\mathbf{k}}^{\text{Tasaki}} = \begin{pmatrix} -2(\cos(k_x) + \cos(k_y)) & a(1 - e^{ik_x}) & a(1 - e^{ik_y}) \\ a(1 - e^{-ik_x}) & a^2 - 4 & 0 \\ a(1 - e^{-ik_y}) & 0 & a^2 - 4 \end{pmatrix}. \quad (\text{S3})$$

In this model, for all  $a$ , there is a lowest isolated flat band at energy  $-4$ , and a flat and dispersive band above the band gap. The band structure is plotted for  $a = 1$ ,  $a = 1.5$  and  $a = 2$  in Fig. S1(c). As  $a$  is increased, the flat and dispersive bands above the flat band of interest shift upwards in energy, but there are no drastic changes in dispersions otherwise. However, condensation rapidly destabilizes when approaching  $a = 2$  due to quantum geometric effects.

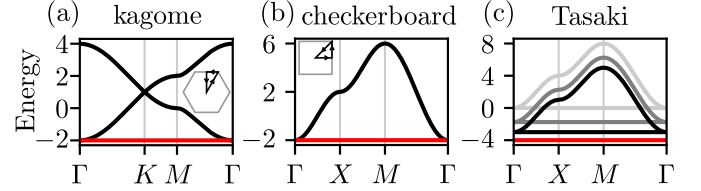


FIG. S1. Band structures of the (a) kagome lattice, (b) checkerboard lattice and (c) modified Tasaki lattice. In the Tasaki lattice, we show band structures for  $a = 1$  (black),  $a = 1.5$  (gray) and  $a = 2$  (light gray). In all panels, the flat band of interest is plotted in red.

### II. DETAILS ON BOGOLIUBOV THEORY

As stated in the main text, we consider the Bose-Hubbard model  $H = H_{\text{kin}} + H_{\text{int}}$ , where

$$H_{\text{kin}} = \sum_{i\alpha,j\beta} b_{i\alpha}^\dagger t_{i\alpha,j\beta} b_{j\beta}, \quad (\text{S4})$$

$$H_{\text{int}} = \frac{U}{2} \sum_{i\alpha} n_{i\alpha}(n_{i\alpha} - 1) - \mu \sum_{i\alpha} n_{i\alpha}.$$

As in the main text,  $b_{i\alpha}$  creates a boson at site  $i\alpha$ ,  $t_{i\alpha,j\beta}$  is the hopping amplitude from site  $j\beta$  to  $i\alpha$ ,  $\mu$  is the chemical potential and  $U$  the on-site repulsive interaction. We consider condensations in a single flat-band eigenstate  $|\varphi_0\rangle$  with  $H_{\text{kin}}|\varphi_0\rangle = \varepsilon_0|\varphi_0\rangle$ . By expanding  $b_{i\alpha} = \sqrt{N_0}\varphi_{i\alpha} + c_{i\alpha}$  and retaining only quadratic terms in the fluctuations  $c_{i\alpha}$ , we obtain

$$\frac{H}{N} = \frac{1}{2N} \boldsymbol{\psi}^\dagger H_B \boldsymbol{\psi} + E_{\text{MF}} + E_0$$

$$H_B = \begin{pmatrix} H_{\text{kin}} - \mu_{\text{eff}} & \Delta \\ \Delta^\dagger & H_{\text{kin}}^* - \mu_{\text{eff}} \end{pmatrix}, \quad \boldsymbol{\psi}^\dagger = (c_{11}^\dagger, \dots, c_{N_c N_b}^\dagger, c_{11}, \dots, c_{N_c N_b}) \quad (\text{S5})$$

$$E_{\text{MF}} = n_0 \langle \varphi_0 | H_{\text{kin}} | \varphi_0 \rangle - n_0 \mu + N \frac{U n_0^2}{2} \sum_{i\alpha} |\varphi_{i\alpha}|^4,$$

$$E_0 = -\frac{1}{2} \text{Tr}[H_{\text{kin}}] + \frac{1}{2} \mu - U n_0,$$

where  $[\Delta]_{i\alpha,j\beta} = U N n_0 \varphi_{i\alpha}^2 \delta_{ij} \delta_{\alpha\beta}$ ,  $[\mu_{\text{eff}}]_{i\alpha,j\beta} = (\mu - 2U N n_0 |\varphi_{i\alpha}|^2) \delta_{i\alpha,j\beta}$ , and  $N_b, N_c$  are the number of bands and unit cells, respectively. The condensate fraction is defined as  $n_0 = N_0/N$ , where  $N_0$  is the number of condensed particles and  $N = N_b N_c$  is the total number of sites.

### A. Minimization of $E_{\text{MF}}$

The state condensation occurs in,  $|\varphi_0\rangle$ , minimizes the mean-field energy  $E_{\text{MF}}$ , with  $\mu$  a Lagrange multiplier enforcing the normalization  $\langle\varphi_0|\varphi_0\rangle = 1$ . In other words, we need to find  $\varphi_{i\alpha}$ ,  $\varphi_{i\alpha}^*$  so that

$$E_{\text{MF}} = n_0 \sum_{i\alpha, j\beta} \varphi_{i\alpha}^* [H_{\text{kin}}]_{i\alpha, j\beta} \varphi_{j\beta} - n_0 \mu \sum_{i\alpha} \varphi_{i\alpha}^* \varphi_{i\alpha} + N \frac{Un_0^2}{2} \sum_{i\alpha} (\varphi_{i\alpha}^*)^2 \varphi_{i\alpha}^2, \quad (\text{S6})$$

is minimized, meaning that  $\varphi_{i\alpha}$  satisfies

$$n_0 \sum_{j\beta} [H_{\text{kin}}]_{i\alpha, j\beta} \varphi_{j\beta} + NU n_0^2 |\varphi_{i\alpha}|^2 \varphi_{i\alpha} - \mu n_0 \varphi_{i\alpha} = 0. \quad (\text{S7})$$

From these relations, we obtain for  $\langle\varphi_0|\varphi_0\rangle = 1$ ,

$$\mu = \langle\varphi_0| H_{\text{kin}} |\varphi_0\rangle + NU n_0 \sum_{i\alpha} |\varphi_{i\alpha}|^4. \quad (\text{S8})$$

When  $|\varphi_0\rangle$  minimizes  $E_{\text{MF}}$ , we can verify that  $\gamma_z H_B (|\varphi_0\rangle, -|\varphi_0^*\rangle)^T = 0$ . Defining the matrix  $[F]_{i\alpha, j\beta} = |\varphi_{i\alpha}|^2 \delta_{i\alpha, j\beta}$ ,

$$\gamma_z H_B \begin{pmatrix} |\varphi_0\rangle \\ -|\varphi_0^*\rangle \end{pmatrix} = \begin{pmatrix} H_{\text{kin}} |\varphi_0\rangle - \mu |\varphi_0\rangle + 2Un_0 F |\varphi_0\rangle - \Delta |\varphi_0^*\rangle \\ H_{\text{kin}}^* |\varphi_0^*\rangle - \mu |\varphi_0^*\rangle + 2Un_0 F |\varphi_0^*\rangle - \Delta^\dagger |\varphi_0\rangle \end{pmatrix}. \quad (\text{S9})$$

Since  $\Delta |\varphi_0^*\rangle = Un_0 F |\varphi_0\rangle$ , the first component can be rewritten as  $(H_{\text{kin}} + Un_0 F) |\varphi_0\rangle - \mu |\varphi_0\rangle$ . On the other hand, Eq. (S7) can be rewritten as  $(H_{\text{kin}} + Un_0 F) |\varphi_0\rangle = \mu |\varphi_0\rangle$ . The first component therefore vanishes. Similarly, the second component of Eq. (S9) also vanishes.

In the main text, we assume  $|\varphi_{i\alpha}| = 1/\sqrt{N}$  is uniform, and that  $|\varphi_0\rangle$  is a flat-band eigenstate with energy  $\varepsilon_0$ . Then

$$\begin{aligned} \mu &= \varepsilon_0 + Un_0, \\ \mu_{\text{eff}} &= \varepsilon_0 - Un_0. \end{aligned} \quad (\text{S10})$$

Note that these expressions coincide with those used in Refs. 32–34, since we define  $n_0$  as the number of condensed particles per site.

### B. Paraunitary standardization and zero-point energy

To determine the eigenmodes of our Hamiltonian, we seek to write  $\psi^\dagger H_B \psi = \gamma^\dagger \varepsilon \gamma$ , where  $\gamma^\dagger = (\gamma_{1+}^\dagger, \dots, \gamma_{N+}^\dagger, \gamma_{1-}, \dots, \gamma_{N-})$  contains Bogoliubov boson operators, and  $\varepsilon$  is diagonal or at least of a form which makes the spectrum clear. To this end, we need to find  $\Gamma$

and  $\varepsilon$  such that  $H_B = \Gamma^\dagger \varepsilon \Gamma$ , meaning that  $\gamma = \Gamma \psi$ . Because the operators  $\gamma$  need to fulfill bosonic commutation relations, we need  $\Gamma \gamma_z \Gamma^\dagger = \gamma_z$ , where  $\gamma_z = \text{diag} \sigma_z \otimes \mathbb{1}_N$ :

$$\begin{aligned} [[\gamma]_i, [\gamma^\dagger]_j] &= [\gamma_z]_{ij} \\ &= \sum_{kl} [\Gamma_{ik} [\psi]_k, [\psi^\dagger]_l \Gamma_{jl}^*] \\ &= \sum_{kl} \Gamma_{ik} [\gamma_z]_{kl} [\Gamma^\dagger]_{lj}. \end{aligned} \quad (\text{S11})$$

In other words, in contrast to fermionic Hamiltonians where it is sufficient to diagonalize  $H_B$ , we need to carry out paraunitary diagonalization (or at least standardization) [68–70]. Now notice that, when  $\Gamma \gamma_z \Gamma^\dagger = \gamma_z$ ,

$$H_B = \Gamma^\dagger \varepsilon \Gamma \Leftrightarrow \Gamma \gamma_z H_B \Gamma^{-1} = \gamma_z \varepsilon, \quad (\text{S12})$$

i.e. we can obtain  $\Gamma$  and  $\varepsilon$  by diagonalizing  $\gamma_z H_B$ , provided it is diagonalizable by a matrix fulfilling  $\Gamma \gamma_z \Gamma^\dagger = \gamma_z$ .

In Bogoliubov theory, this is unfortunately not quite the case: the matrix  $\gamma_z H_B$  has a vanishing eigenvalue with a geometric multiplicity of one and an algebraic multiplicity of two, meaning it is not diagonalizable. In this case, it is impossible to find a diagonal  $\varepsilon$  while keeping the components of  $\Gamma$  finite. However, it is possible to keep  $\Gamma$  finite if we allow  $\varepsilon$  to have the nondiagonal standard form [69, 70]:

$$\varepsilon = \begin{pmatrix} \varepsilon_{>0} & 0 & 0 & 0 \\ 0 & \mathbb{1}_{n_{\text{zeros}}} & 0 & J \\ 0 & 0 & \varepsilon_{>0} & 0 \\ 0 & J & 0 & \mathbb{1}_{n_{\text{zeros}}} \end{pmatrix}, \quad (\text{S13})$$

where  $\varepsilon_{>0}$  is a diagonal matrix containing the eigenvalues with equal geometric and algebraic multiplicity (in our case, nonzero eigenvalues) and  $n_{\text{zeros}}$  is the number of improper zero modes (in Bogoliubov theory,  $n_{\text{zeros}} = 1$ ). The matrix  $J$  is diagonal with  $[J]_{ii} \equiv \eta_i$ , with each  $\eta_i$  either 1 or  $-1$ .

Hamiltonians in this standardized form have a known spectrum [70], and the zero-point energy of  $\psi^\dagger H_B \psi$  coincides with the zero-point energy of

$$\begin{aligned} &\sum_{i=1}^{N-n_{\text{zeros}}} \varepsilon_i (\gamma_{i+}^\dagger \gamma_{i+} + \gamma_{i-} \gamma_{i-}^\dagger) \\ &= \sum_{i=1}^{N-n_{\text{zeros}}} \varepsilon_i (\gamma_{i+}^\dagger \gamma_{i+} + \gamma_{i-}^\dagger \gamma_{i-}) + \sum_{i=1}^{N-n_{\text{zeros}}} \varepsilon_i. \end{aligned} \quad (\text{S14})$$

The zero-point energy for the Hamiltonian  $\psi^\dagger H_B \psi$  is therefore  $\sum_{i=1}^{N-n_{\text{zeros}}} \varepsilon_i$ .

The full Hamiltonian considered in this work is

$$\frac{H}{N} = \frac{1}{2N} \psi^\dagger H_B \psi + E_{\text{MF}} + E_0. \quad (\text{S15})$$

Since  $|\varphi_0\rangle$  minimizes the mean-field energy  $E_{\text{MF}}$  and is a flat-band eigenstate,  $E_{\text{MF}}$  and  $E_0$  are independent of the

particular  $|\varphi_0\rangle$ . We therefore define the zero-point energy as

$$\Lambda = \frac{1}{2N} \sum_n \varepsilon_n, \quad (\text{S16})$$

where the sum runs over the strictly positive eigenvalues of  $\gamma_z H_B$ . This is the definition used in the main text.

### 1. Numerical diagonalization of $\gamma_z H_B$

The diagonalization of  $\gamma_z H_B$  can in principle be performed directly, with the caveat that it is not diagonalizable on the eigenspace of zero modes. However, especially in the presence of degenerate nonzero eigenvalues, the eigenvectors might require further processing to fulfill the required condition  $\Gamma \gamma_z \Gamma^\dagger = \gamma_z$ . To circumvent this issue, we employ the method proposed in Ref. 68, which requires no diagonalization of non-Hermitian matrices and always provides a  $\Gamma$  fulfilling  $\Gamma \gamma_z \Gamma^\dagger = \gamma_z$ . Reference 68 mostly covers cases where  $H_B$  is positive definite, which is not the case here. However, treating a positive semidefinite  $H_B$  as the limit of a positive definite matrix allows us to obtain eigenvectors corresponding to eigenvalues which remain nonzero in this limit. We do not need knowledge of the zero modes, but they can be determined using an algorithm proposed in Refs. [69, 70].

When eigenvectors are needed, we use the following procedure:

1. We add a small positive shift to make  $H_B$  positive definite,  $\tilde{H}_B = H_B + \epsilon \mathbb{1}_{2N}$ . This allows us to determine a Cholesky decomposition of  $\tilde{H}_B = \mathcal{K}^\dagger \mathcal{K}$ .
2. We construct the Hermitian matrix  $\tilde{G} = \mathcal{K} \gamma_z \mathcal{K}^\dagger$ , and diagonalize it to obtain  $\tilde{G} = \mathcal{U} \mathcal{L} \mathcal{U}^\dagger$ , where  $\mathcal{U}$  is a unitary matrix and  $\mathcal{L}$  is a diagonal matrix with an equal number of positive and negative entries. We order the entries in  $\mathcal{L}$  so that the first  $N$  are positive, and the last  $N$  are negative. We then take  $\varepsilon = \gamma_z \mathcal{L}$ , which only contains positive entries.

3. We now take  $\Gamma = (\gamma_z \mathcal{L})^{-1/2} \mathcal{U}^\dagger \mathcal{K}$ . We can verify that

$$\begin{aligned} \Gamma \gamma_z \Gamma^\dagger &= (\gamma_z \mathcal{L})^{-1/2} \mathcal{U}^\dagger \mathcal{K} \gamma_z \mathcal{K}^\dagger \mathcal{U} (\gamma_z \mathcal{L})^{-1/2} \\ &= (\gamma_z \mathcal{L})^{-1/2} \mathcal{U}^\dagger (\mathcal{U} \mathcal{L} \mathcal{U}^\dagger) \mathcal{U} (\gamma_z \mathcal{L})^{-1/2} \\ &= \gamma_z, \\ \Gamma^\dagger \varepsilon \Gamma &= \mathcal{K}^\dagger \mathcal{U} (\gamma_z \mathcal{L})^{-1/2} (\gamma_z \mathcal{L}) (\gamma_z \mathcal{L})^{-1/2} \mathcal{U}^\dagger \mathcal{K} \\ &= \mathcal{K}^\dagger \mathcal{K} = H_B + \epsilon \mathbb{1}_{2N}. \end{aligned} \quad (\text{S17})$$

By taking  $\epsilon$  small enough, we can obtain the eigenvalues and eigenvectors corresponding to nonzero eigenvalues of  $\gamma_z H_B$  using this method, without diagonalizing a non-hermitian matrix. However, this method often turns out to be slower than the direct diagonalization of  $\gamma_z H_B$ , and we therefore use it only when eigenvectors are required.

## C. Computation of $n_0$

We compute  $n_0$  self-consistently. We start from an initial guess for  $n_0$ , and construct the Hamiltonian  $H_B$  with this value. We then evaluate the excitation fraction  $n_{\text{ex}}$ , and use that  $n_{\text{tot}} = n_0 + n_{\text{ex}}$  to obtain a new value for  $n_0$ . We reconstruct  $H_B$  with this new value and repeat the procedure until  $n_0$  has converged. Note that  $|\varphi_0\rangle$  is not updated during this procedure, since on a flat band the set of wavefunctions minimizing the mean-field energy does not depend on  $n_0$ .

The excitation fraction can be computed from the matrices  $\varepsilon$  and  $\Gamma$  obtained as a result of the paraunitary standardization:

$$\begin{aligned} n_{\text{ex}} &= \frac{1}{N} \sum'_{i\alpha} \langle c_{i\alpha}^\dagger c_{i\alpha} \rangle = \frac{1}{2N} \sum'_{i\alpha} \left( \langle c_{i\alpha}^\dagger c_{i\alpha} \rangle + \langle c_{i\alpha} c_{i\alpha}^\dagger \rangle - 1 \right) \\ &= \frac{1}{2N} \sum'_{i\alpha} \left( \langle [\psi^\dagger]_i, [\psi]_i \rangle - 1 \right) \\ &= \frac{1}{2N} \sum'_{ijk} \left( [(\Gamma^{-1})^\dagger]_{ji} [\Gamma^{-1}]_{ik} \langle [\gamma^\dagger]_j [\gamma]_k \rangle - 1 \right), \end{aligned} \quad (\text{S18})$$

where  $\sum'$  indicates that the zero modes should be excluded from the summation.

For a more convenient notation, we can define  $|\psi_{n+}\rangle$  the  $n$ :th column of  $\Gamma^{-1}$  and  $|\psi_{n-}\rangle$  the  $n+N$ :th column. Then, since the Bogoliubov bosons follow bosonic statistics, we obtain at zero temperature that

$$n_{\text{ex}} = \frac{1}{2N} \sum_{n=1}^{N-n_{\text{zeroes}}} (-1 + \langle \psi_{n-} | \psi_{n-} \rangle). \quad (\text{S19})$$

To determine  $n_0$ , we therefore need the eigenvectors corresponding to strictly negative eigenvalues of  $\gamma_z H_B$ .

## III. ROLE OF NON-CONTRACTIBLE LOOP STATES

In the main text, we considered constraints imposed by the overlap of CLSs at sites which do not involve the NLSs in our basis. As the system size increases, most sites will usually not be occupied by an NLS, but they play an important role in systems with periodic boundary conditions. To illustrate this, we consider a  $3 \times 3$  unit cell kagome lattice with periodic boundary conditions.

In the kagome lattice, the overlaps, or absence thereof, at the sites which do not involve an NLS (see Fig. S2a) impose the following constraints for a uniform  $|\varphi_{i\alpha}\rangle$ :

1.  $|\omega_5| = |\omega_8| = 1/\sqrt{N}$  from the sites which do not have overlaps due to the plaquette which has no associated CLS (the CLS on this plaquette can be constructed from the other CLSs and NLSs, and is therefore not needed),

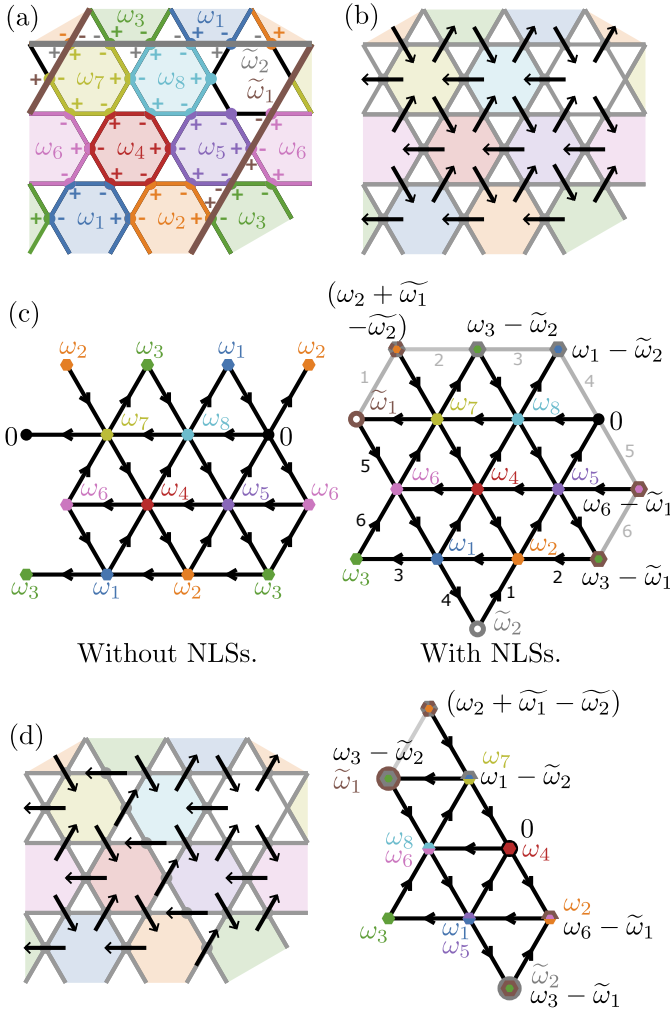


FIG. S2. (a) Possible choice of basis of CLSs and NLSs in a kagome lattice with periodic boundary conditions and  $3 \times 3$  unit cells. (b) Wavefunction corresponding to the  $\mathbf{k} = (0,0)$  Bloch function. Each arrow represents the complex number  $\varphi_{i\alpha}$  and has length  $1/\sqrt{N}$ . (c) Left: Coefficients  $\omega_i$  corresponding to the wavefunction in (b) when NLSs are not included. Some points, such as  $\omega_1, \omega_2, \omega_3$  and even 0 would need to be at several distinct positions in the complex plane to reproduce the desired phase pattern: the wavefunction in (b) can not be constructed from CLSs alone. Right: Configuration of coefficients when NLSs are also included. In this case, coefficients are well-defined, and some vertices of the framework correspond to linear combination of the various coefficients instead of the coefficients themselves. Note that because of periodic boundary conditions, the numbered black edges need to match the direction of the corresponding numbered gray edges. (d) Example of another candidate wavefunction, which is not a Bloch function, and can only be constructed by allowing for nonzero  $\tilde{\omega}_1$  and  $\tilde{\omega}_2$ .

2.  $|\omega_i - \omega_j| = 1/\sqrt{N}$  for the pairs  $\{i, j\} = \{1, 2\}, \{1, 3\}, \{1, 4\}, \{1, 6\}, \{2, 4\}, \{2, 5\}, \{3, 6\}, \{4, 5\}, \{4, 6\}, \{4, 7\}, \{4, 8\}, \{5, 8\}, \{6, 7\}, \{7, 8\}$ .

From the sites which involve NLSs, on the other hand, we get

3.  $|\omega_i - \tilde{\omega}_2| = |\omega_2 - \tilde{\omega}_2| = |\omega_6 - \tilde{\omega}_1| = |\omega_7 - \tilde{\omega}_1| = 1/\sqrt{N}$  from sites surrounding the plaquette without an associated CLS,
4.  $|\omega_2 + \tilde{\omega}_1 - \omega_7 - \tilde{\omega}_2| = 1/\sqrt{N}$  from the site where the two NLSs cross,
5.  $|\omega_i - \omega_j - \tilde{\omega}_1| = 1/\sqrt{N}$  for  $\{i, j\} = \{2, 3\}, \{5, 3\}, \{5, 6\}$ , and  $|\omega_i - \omega_j - \tilde{\omega}_2| = 1/\sqrt{N}$  for  $\{i, j\} = \{3, 7\}, \{3, 8\}, \{1, 8\}$  from the other sites.

In total, this gives 27 constraints on the positions of  $\omega_i$  and  $\tilde{\omega}_i$  in the complex plane, one for each site. In the absence of NLSs, i.e. setting  $\tilde{\omega}_i = 0$ , the Bloch function corresponding to  $\mathbf{k} = (0,0)$ , shown in Fig. S2(b), could not be constructed. However, this is possible to achieve once NLSs are also included (see Fig. S2(c)). This is expected, since  $\mathbf{k} = (0,0)$  has a singular band touching, which necessitates the inclusion of NLSs.

If NLSs are not included, problems can occur also for states that are not simply Bloch functions but involve the  $\mathbf{k} = (0,0)$ , as shown in Fig. S2(d).

#### IV. VERIFYING STABILITY WITHOUT EXPLICITLY CONSIDERING FRAMEWORKS

A particular  $|\varphi_0\rangle$  is a flat-band eigenstate if and only if

$$|\varphi_0\rangle = T\boldsymbol{\omega}, \quad (\text{S20})$$

where  $\boldsymbol{\omega} = (\omega_1, \dots, \omega_{n_{\text{CLS}}}, \tilde{\omega}_1, \dots, \tilde{\omega}_{n_{\text{NLS}}})$ , with  $n_{\text{CLS}}$  and  $n_{\text{NLS}}$  the numbers of CLSs and NLSs, respectively. The matrix  $T$  is of dimension  $N \times (n_{\text{CLS}} + n_{\text{NLS}})$ , with  $[T]_{i\alpha, j} = \nu(\mathbf{R}_j - \mathbf{R}_i)_\alpha$ ,  $j = 1, \dots, n_{\text{CLS}}$ , the amplitude of the  $j$ :th CLS at site  $i\alpha$ , and  $[T]_{i\alpha, j+n_{\text{CLS}}} = \tilde{\nu}_{i\alpha, j}$ ,  $j = 1, \dots, n_{\text{NLS}}$  the amplitude of the  $j$ :th NLS at site  $i\alpha$ .

For a particular candidate wavefunction  $|\varphi_0\rangle$ , Eq. (S20) has nontrivial solutions  $\boldsymbol{\omega}$  if and only if  $TT^+|\varphi_0\rangle = |\varphi_0\rangle$ , where  $T^+$  is the Moore-Penrose pseudoinverse of  $T$ . A nontrivial solution  $\boldsymbol{\omega}$  also exists if and only if  $|\varphi_0\rangle$  can be constructed from the CLSs and NLSs, meaning it is a flat-band eigenstate. We assume this is the case for some  $|\varphi_0\rangle$  with uniform  $|\varphi_{i\alpha}|$ .

A stable condensate is impossible in  $|\varphi_0\rangle$  if there exists a pair of flat-band states  $C|\varphi_0\rangle, C^\dagger|\varphi_0\rangle$  where  $C$  is a diagonal matrix (or a single flat-band state  $C|\varphi_0\rangle$  when  $C$  is real). In order for stable condensation to be possible, there should therefore exist no  $C$  not proportional to identity such that  $TT^+C|\varphi_0\rangle = C|\varphi_0\rangle$  and  $TT^+C^\dagger|\varphi_0\rangle = C^\dagger|\varphi_0\rangle$  simultaneously.

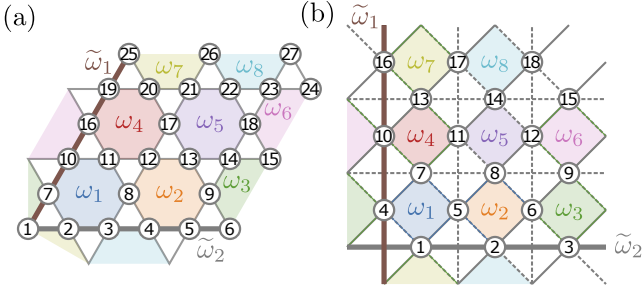


FIG. S3. Numbering of sites and CLSs/NLSs used in the (a) kagome and (b) checkerboard lattice when building the matrix  $T$  (see Eq. (S20)).

Let us now define a diagonal unitary matrix  $[A]_{i\alpha,j\beta} = e^{i\theta_{i\alpha}} \delta_{i\alpha,j\beta}$ , so that  $|\varphi_0\rangle = A|u\rangle$ , with  $|u\rangle = (1, \dots, 1)/\sqrt{N}$  a real vector. Then  $G|u\rangle = |u\rangle$ , where  $G = A^\dagger T T^\dagger A$  is a Hermitian matrix. If a pair of states  $C|\varphi_0\rangle$  and  $C^\dagger|\varphi_0\rangle$  exists on the flat band,  $G|v\rangle = |v\rangle$  and  $G|v^*\rangle = |v^*\rangle$ , where  $|v\rangle = C|u\rangle$ , i.e.  $G$  has a corresponding eigenvector corresponding to a unit eigenvalue such that its complex conjugate is also an eigenvector of  $G$  corresponding to a unit eigenvalue. Conversely, if there exists a vector  $|x\rangle$  such that  $G|x\rangle = |x\rangle$  and  $G|x^*\rangle = |x^*\rangle$  simultaneously, we can define  $[U]_{i\alpha,i\alpha} = \arg[|x\rangle]_{i\alpha}$  and  $[R] = \sqrt{N}|[|x\rangle]_{i\alpha}|$  to recover a pair of states  $A|x\rangle = RU|\varphi_0\rangle$  and  $A|x^*\rangle = RU^\dagger|\varphi_0\rangle$ . A pair of states  $C|\varphi_0\rangle$ ,  $C^\dagger|\varphi_0\rangle$  therefore exists on the flat band if and only if  $G$  has a corresponding eigenvector with unit eigenvalue such that its complex conjugate is also an eigenvector of  $G$  with unit eigenvalue.

Such vectors are simultaneous eigenvectors of  $G$  and  $G^*$ . For stable condensation to be possible, we therefore need  $G$  and  $G^*$  to have exactly one simultaneous eigenvector corresponding to a unit eigenvalue,  $|u\rangle$ . In other words, the intersection  $V = \ker[G - \mathbb{1}] \cap \ker[G^* - \mathbb{1}]$  should be one-dimensional for stable condensation to be possible.

Note that for a large system, because of the translational invariance, it is usually sufficient to consider a system of fewer unit cells to verify that the set of CLSs and NLSs is compatible with a stable BEC.

#### A. Example: kagome lattice

In the kagome lattice, using the numbering shown in Fig. S3(a), a possible matrix  $T$  for a system of  $3 \times 3$  unit

cells is

$$T = \begin{pmatrix} 0 & 0 & -1 & 0 & 0 & 0 & +1 & 0 & -1 & +1 \\ +1 & 0 & 0 & 0 & 0 & 0 & 0 & -1 & 0 & 0 & -1 \\ -1 & 0 & 0 & 0 & 0 & 0 & 0 & 0 & +1 & 0 & +1 \\ 0 & +1 & 0 & 0 & 0 & 0 & 0 & 0 & -1 & 0 & -1 \\ 0 & -1 & 0 & 0 & 0 & 0 & 0 & 0 & 0 & 0 & +1 \\ 0 & 0 & +1 & 0 & 0 & 0 & 0 & 0 & 0 & 0 & -1 \\ -1 & 0 & +1 & 0 & 0 & 0 & 0 & 0 & 0 & +1 & 0 \\ +1 & -1 & 0 & 0 & 0 & 0 & 0 & 0 & 0 & 0 & 0 \\ 0 & +1 & -1 & 0 & 0 & 0 & 0 & 0 & 0 & 0 & 0 \\ +1 & 0 & 0 & 0 & 0 & -1 & 0 & 0 & 0 & -1 & 0 \\ -1 & 0 & 0 & +1 & 0 & 0 & 0 & 0 & 0 & 0 & 0 \\ 0 & +1 & 0 & -1 & 0 & 0 & 0 & 0 & 0 & 0 & 0 \\ 0 & -1 & 0 & 0 & +1 & 0 & 0 & 0 & 0 & 0 & 0 \\ 0 & 0 & +1 & 0 & -1 & 0 & 0 & 0 & 0 & 0 & 0 \\ 0 & 0 & -1 & 0 & 0 & +1 & 0 & 0 & 0 & 0 & 0 \\ 0 & 0 & 0 & -1 & 0 & +1 & 0 & 0 & +1 & 0 & 0 \\ 0 & 0 & 0 & +1 & -1 & 0 & 0 & 0 & 0 & 0 & 0 \\ 0 & 0 & 0 & 0 & +1 & -1 & 0 & 0 & 0 & 0 & 0 \\ 0 & 0 & 0 & +1 & 0 & 0 & 0 & 0 & 0 & -1 & 0 \\ 0 & 0 & 0 & -1 & 0 & 0 & +1 & 0 & 0 & 0 & 0 \\ 0 & 0 & 0 & 0 & +1 & 0 & -1 & 0 & 0 & 0 & 0 \\ 0 & 0 & 0 & 0 & 0 & +1 & 0 & -1 & 0 & 0 & 0 \\ 0 & 0 & 0 & 0 & 0 & -1 & 0 & 0 & 0 & 0 & 0 \\ 0 & 0 & 0 & 0 & 0 & 0 & -1 & 0 & +1 & 0 & 0 \\ 0 & 0 & 0 & 0 & 0 & 0 & +1 & -1 & 0 & 0 & 0 \\ 0 & 0 & 0 & 0 & 0 & 0 & 0 & +1 & 0 & 0 & 0 \end{pmatrix} \quad (\text{S21})$$

We can verify for instance the stability of condensation into the  $\mathbf{k} = (0, 0)$  state

$$|\varphi_0\rangle = \frac{1}{\sqrt{N}} (e^{-i\frac{\pi}{3}}, e^{i\frac{\pi}{3}}, e^{-i\frac{\pi}{3}}, e^{i\frac{\pi}{3}}, e^{-i\frac{\pi}{3}}, e^{i\frac{\pi}{3}}, -1, -1, -1, e^{-i\frac{\pi}{3}}, e^{i\frac{\pi}{3}}, e^{-i\frac{\pi}{3}}, e^{i\frac{\pi}{3}}, e^{-i\frac{\pi}{3}}, e^{i\frac{\pi}{3}}, -1, -1, -1, e^{-i\frac{\pi}{3}}, e^{i\frac{\pi}{3}}, e^{-i\frac{\pi}{3}}, e^{i\frac{\pi}{3}}, e^{-i\frac{\pi}{3}}, e^{i\frac{\pi}{3}}, -1, -1, -1)^T. \quad (\text{S22})$$

We numerically solve for  $V = \ker[G - \mathbb{1}] \cap \ker[G^* - \mathbb{1}]$ , and find that it is one-dimensional (spanned by a vector with all entries equal), meaning that for this  $|\varphi_0\rangle$ , the condensate can be stable.

#### B. Example: checkerboard lattice

In the checkerboard lattice considered in the main text, we again consider a  $3 \times 3$  unit cell system, and use the

numbering shown in Fig. S3(b) to obtain

$$T = \begin{pmatrix} -1 & 0 & 0 & 0 & 0 & 0 & 0 & +1 & 0 & +1 & 0 \\ 0 & -1 & 0 & 0 & 0 & 0 & 0 & 0 & +1 & +1 & 0 \\ 0 & 0 & -1 & 0 & 0 & 0 & 0 & 0 & 0 & +1 & 0 \\ -1 & 0 & +1 & 0 & 0 & 0 & 0 & 0 & 0 & 0 & +1 \\ +1 & -1 & 0 & 0 & 0 & 0 & 0 & 0 & 0 & 0 & 0 \\ 0 & +1 & -1 & 0 & 0 & 0 & 0 & 0 & 0 & 0 & 0 \\ +1 & 0 & 0 & -1 & 0 & 0 & 0 & 0 & 0 & 0 & 0 \\ 0 & +1 & 0 & 0 & -1 & 0 & 0 & 0 & 0 & 0 & 0 \\ 0 & 0 & +1 & 0 & 0 & -1 & 0 & 0 & 0 & 0 & 0 \\ 0 & 0 & 0 & -1 & 0 & +1 & 0 & 0 & 0 & 0 & +1 \\ 0 & 0 & 0 & +1 & -1 & 0 & 0 & 0 & 0 & 0 & 0 \\ 0 & 0 & 0 & 0 & +1 & -1 & 0 & 0 & 0 & 0 & 0 \\ 0 & 0 & 0 & +1 & 0 & 0 & -1 & 0 & 0 & 0 & 0 \\ 0 & 0 & 0 & 0 & +1 & 0 & 0 & -1 & 0 & 0 & 0 \\ 0 & 0 & 0 & 0 & 0 & +1 & 0 & 0 & 0 & 0 & 0 \\ 0 & 0 & 0 & 0 & 0 & 0 & -1 & 0 & 0 & +1 & 0 \\ 0 & 0 & 0 & 0 & 0 & 0 & +1 & -1 & 0 & 0 & 0 \\ 0 & 0 & 0 & 0 & 0 & 0 & 0 & +1 & 0 & 0 & 0 \end{pmatrix} \quad (\text{S23})$$

A flat-band eigenstate with uniform  $|\varphi_{i\alpha}|$  is

$$|\varphi_0\rangle = (1, 1, 1, i, i, i, \\ 1, 1, 1, i, i, i, \\ 1, 1, 1, i, i, i)^T. \quad (\text{S24})$$

In this case,  $V$  is six-dimensional, spanned by six real vectors

$$\begin{aligned} v_1 &= (1, 1, 1, 0, 0, 0, 0, 0, 0, 0, 0, 0, 0, 0, 0, 0)^T, \\ v_2 &= (0, 0, 0, 0, 0, 0, 1, 1, 1, 0, 0, 0, 0, 0, 0, 0)^T, \\ v_3 &= (0, 0, 0, 0, 0, 0, 0, 0, 0, 0, 0, 0, 1, 1, 1, 0)^T, \\ v_4 &= (0, 0, 0, 1, 0, 0, 0, 0, 0, 1, 0, 0, 0, 0, 0, 1)^T, \\ v_5 &= (0, 0, 0, 0, 1, 0, 0, 0, 0, 0, 1, 0, 0, 0, 0, 1)^T, \\ v_6 &= (0, 0, 0, 0, 0, 1, 0, 0, 0, 0, 0, 1, 0, 0, 0, 0)^T. \end{aligned} \quad (\text{S25})$$

The condensate is therefore unstable.

### C. Example: Tasaki lattice

Here we consider two values of  $a$  compatible with periodic boundary conditions and a system size of  $4 \times 4$  unit cells:  $a = \sqrt{2}$  and  $a = 2$ . Since the matrix  $T$  has dimensions  $48 \times 16$ , we do not provide it explicitly. In the  $a = \sqrt{2}$  case, picking  $|\varphi_0\rangle$  as the Bloch function corresponding to  $\mathbf{k} = (\pi/2, \pi/2)$ , we find that  $V$  is a one-dimensional vector space. For  $a = 2$ ,  $|\varphi_0\rangle$  is the Bloch function at  $\mathbf{k} = (\pi, \pi)$ , and  $V$  turns out to be a 16-dimensional vector space. At  $a = 2$ , the condensate is thus unstable, while it can be stable for  $a = \sqrt{2}$ .

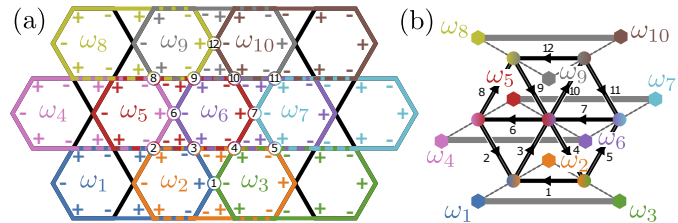


FIG. S4. (a) One possible choice of CLSs in the kagome lattice. Each CLS occupies two horizontally adjacent hexagonal plaquettes. We do not show all CLSs and NLSs, but instead focus on the constraints imposed by the overlaps at the 12 numbered sites. (b) One configuration of the coefficients  $\omega_i$  corresponding to uniform densities. The single-colored hexagons represent the coefficients  $\omega_i$ , while circles colored by gradients are the middle point of the dashed lines they are on (i.e. they are midpoints  $(\omega_i + \omega_j)/2$ ). The thick gray lines have a length of  $1/\sqrt{N}$ . The black arrows have length  $1/(2\sqrt{N})$ , and each corresponds to  $\varphi_i/2$ , with  $i = 1 \dots 12$  one of the sites. The length of the dashed lines is not fixed, and the positions of  $\omega_i$  can thus be continuously modified; however, the midpoints need to lie on a triangular framework, the edges of which correspond to  $\varphi_i/2$ .

### V. BASIS-INDEPENDENCE OF THE STABILITY

Since the approach outlined in this work relies on finding uniform-density states  $|\varphi_0\rangle$  and verifying that no states  $C|\varphi_0\rangle$ ,  $C^\dagger|\varphi_0\rangle$  exist on the flat band, the results should clearly be independent of the choice of CLSs and NLSs: no matter the basis, the states on the flat band should be the same. Although picking a basis with more complicated CLSs can make the constraints on  $\omega_i$  more difficult to interpret geometrically, the choice of CLSs indeed does not matter for conclusions regarding possible  $|\varphi_0\rangle$  and whether condensation is possible in them.

As an example, let us consider the kagome lattice. In the main text, we showed that all uniform-density states can be represented by a triangular framework, with each  $\varphi_{i\alpha}$  corresponding to one edge of an equilateral triangle. Let us now consider a different choice of CLSs, and show that it leads to the same conclusion. Instead of CLSs occupying one hexagonal plaquette each, we choose CLSs occupying two adjacent plaquettes (see Fig. S4(a)). Because of this choice, there are now sites at which four CLSs overlap, which complicates the constraints slightly. From the overlaps at the numbered sites in Fig. S4(a), we obtain the following constraints:

1. Sites 1, 6, 7 and 12:  $|\omega_i - \omega_j| = 1/\sqrt{N}$  for  $\{i, j\} = \{1, 3\}, \{4, 6\}, \{5, 7\}, \{8, 10\}$ . This simply means that the coefficients in these pairs are a distance of  $1/\sqrt{N}$  away from each other in the complex plane.
2. Sites 2, 3, 4, 5, 8, 9, 10 and 11:  $|\omega_i + \omega_j - \omega_k - \omega_l| = 1/\sqrt{N}$  for  $\{i, j, k, l\} = \{1, 2, 4, 5\}, \{1, 2, 5, 6\}, \{2, 3, 5, 6\}, \{2, 3, 6, 7\}, \{4, 5, 8, 9\}, \{5, 6, 8, 9\}, \{5, 6, 9, 10\}, \{6, 7, 9, 10\}$ . For an easier geometric

interpretation, it is convenient to rewrite the constraint as

$$\left| \frac{\omega_i + \omega_j}{2} - \frac{\omega_k + \omega_l}{2} \right| = \frac{1}{2\sqrt{N}}, \quad (\text{S26})$$

meaning that the middle of the line between  $\omega_i$  and  $\omega_j$  is at a distance of  $1/(2\sqrt{N})$  from the middle of the line between  $\omega_k$  and  $\omega_l$ .

To understand how these constraints come together, notice that

$$\frac{1}{2}(\omega_i + \omega_j) - \frac{1}{2}(\omega_j + \omega_k) = \frac{1}{2}(\omega_i - \omega_k). \quad (\text{S27})$$

Now consider the case  $i = 1$ ,  $j = 2$  and  $k = 3$ . We know the distance between  $\omega_1$  and  $\omega_3$  is  $1/\sqrt{N}$  by the first set of constraints. Then the distance between  $(\omega_1 + \omega_2)/2$  and  $(\omega_2 + \omega_3)/2$  is  $1/(2\sqrt{N})$ . Moreover, since  $\omega_1 - \omega_3 = \varphi_1$ ,  $(\omega_1 + \omega_2)/2 - (\omega_2 + \omega_3)/2 = \varphi_1/2$ .

From the constraint from site 3, we also know that the distance between  $(\omega_1 + \omega_2)/2$  and  $(\omega_5 + \omega_6)/2$  is  $1/(2\sqrt{N})$ . Similarly, it follows from the constraint from site 4 that the distance between  $(\omega_2 + \omega_3)/2$  and  $(\omega_5 + \omega_6)/2$  is  $1/(2\sqrt{N})$ . Therefore  $(\omega_1 + \omega_2)/2$ ,  $(\omega_2 + \omega_3)/2$  and  $(\omega_5 + \omega_6)/2$  need to form an equilateral triangle with side length  $1/(2\sqrt{N})$ . Applying a similar reasoning, we can also deduce that the sets

$$\begin{aligned} & \{(\omega_4 + \omega_5)/2, (\omega_5 + \omega_6)/2, (\omega_1 + \omega_2)/2\}, \\ & \{(\omega_5 + \omega_6)/2, (\omega_6 + \omega_7)/2, (\omega_2 + \omega_3)/2\}, \\ & \{(\omega_4 + \omega_5)/2, (\omega_5 + \omega_6)/2, (\omega_8 + \omega_9)/2\}, \\ & \{(\omega_8 + \omega_9)/2, (\omega_9 + \omega_{10})/2, (\omega_5 + \omega_6)/2\}, \\ & \{(\omega_5 + \omega_6)/2, (\omega_6 + \omega_7)/2, (\omega_9 + \omega_{10})/2\} \end{aligned} \quad (\text{S28})$$

all form equilateral triangles in the complex plane (see Fig. S4). Each of the sides of these equilateral triangles corresponds to  $\varphi_i/2$  for one of the sites of the lattice, and all possible uniform-density eigenstates are three-colorings of the kagome lattice (there are only three distinct orientations for the sides of the triangles, and adjacent edges of a triangle need to have distinct orientations).

With this other choice of CLSs, the obtained set of wavefunctions is thus the same as for the choice used in the main text, as it should. The difference is that for the simpler choice of basis used in the main text, each vertex of the triangular framework representing  $|\varphi_0\rangle$  corresponds to a coefficient  $\omega_i$ , while for the more complicated choice used here, each vertex instead corresponds to a linear combination  $(\omega_i + \omega_j)/2$ , with  $i$  and  $j$  corresponding to adjacent plaquettes.

## VI. STABILITY OF TRIANGULATED FRAMEWORKS

We argue here that if a flat-band state  $|\varphi_0\rangle$  is represented by a triangulated framework (i.e. each edge of a

triangulated framework corresponds to  $b_{i\alpha}\varphi_{i\alpha}$ ), there can exist no states  $R|\varphi_0\rangle$  or pairs of states  $RU|\varphi_0\rangle$ ,  $RU^\dagger|\varphi_0\rangle$  on the flat band, with  $R$  a real diagonal matrix and  $U$  a diagonal unitary matrix. Note that we assume here that each triangle in the framework has nonzero area.

Let us first consider the possibility of a pair of states  $RU|\varphi_0\rangle$ ,  $RU^\dagger|\varphi_0\rangle$ , with  $U$  a diagonal unitary matrix. Let us start by considering a single triangle in the triangulated framework corresponding to  $|\varphi_0\rangle$ . The corresponding triangles in  $RU|\varphi_0\rangle$  and  $RU^\dagger|\varphi_0\rangle$  have identical edge lengths, because  $U$  only changes angles. These two triangles are thus related by rotations and/or reflections.

First, let us consider the case where the two triangles are related by a single reflection. We label 1, 2, 3 the corners of the original triangle in  $|\varphi_0\rangle$ , 1', 2', 3' the corners of the triangle in  $RU|\varphi_0\rangle$  and 1'', 2'', 3'' the corners of the triangle in  $RU^\dagger|\varphi_0\rangle$ . Let us focus on the edges between (1, 2), (1', 2') and (1'', 2''). By assumption, if (1', 2') is rotated by an angle  $\theta$  compared to (1, 2), (1'', 2'') is rotated by an angle  $-\theta$  compared to (1, 2). This is only possible if (1, 2) is parallel to the reflection line between the triangles (1', 2', 3') and (1'', 2'', 3''). The same reasoning can be used for the edges (1, 3) and (2, 3). All three edges of the triangle (1, 2, 3) thus need to be parallel to each other when (1', 2', 3') and (1'', 2'', 3'') are related by a reflection. This goes against the assumption of a nonzero surface area, and corresponding triangles in  $RU|\varphi_0\rangle$  and  $RU^\dagger|\varphi_0\rangle$  can not be related by a reflection.

Corresponding triangles in  $RU|\varphi_0\rangle$ ,  $RU^\dagger|\varphi_0\rangle$  are therefore related by at most an overall rotation. Now consider an adjacent triangle to the one originally considered. Again, the corresponding triangles in  $RU|\varphi_0\rangle$  and  $RU^\dagger|\varphi_0\rangle$  need to be related by an overall rotation. Because these triangles share an edge with the first triangle we considered, this rotation needs to be the same as for the first triangle. Using the same reasoning for all triangles, we get that  $RU|\varphi_0\rangle$  and  $RU^\dagger|\varphi_0\rangle$  need to be related by an overall rotation, i.e.  $U$  can only be a gauge transformation.

It remains to show that there can exist no states  $R|\varphi_0\rangle$  on the flat band. Such state would correspond to a framework with the same connectivity as  $|\varphi_0\rangle$ , with all edges parallel to those in  $|\varphi_0\rangle$ . First, consider a single triangle in  $|\varphi_0\rangle$ , and the corresponding triangle in  $|\varphi'_0\rangle = R|\varphi_0\rangle$ . Since all edges of these triangles are parallel, the two triangles are similar (assuming the triangles have nonzero area). This means that all edges are scaled by the same factor  $c$ . Now consider a triangle that shares an edge with this first triangle: again, these triangles in  $|\varphi_0\rangle$  and  $R|\varphi_0\rangle$  need to be similar. Since one edge of the triangle in  $R|\varphi_0\rangle$  is scaled by  $c$  compared to the corresponding edge in  $|\varphi_0\rangle$ , all edges need to be scaled by  $c$ . By the same reasoning, it follows that all edges in  $R|\varphi_0\rangle$  need to be scaled by the same factor  $c$  to keep the edges parallel to those in  $|\varphi_0\rangle$ :  $R$  is proportional to the identity and  $|\varphi_0\rangle$  and  $R|\varphi_0\rangle$  are the same state up to a gauge transformation and possibly

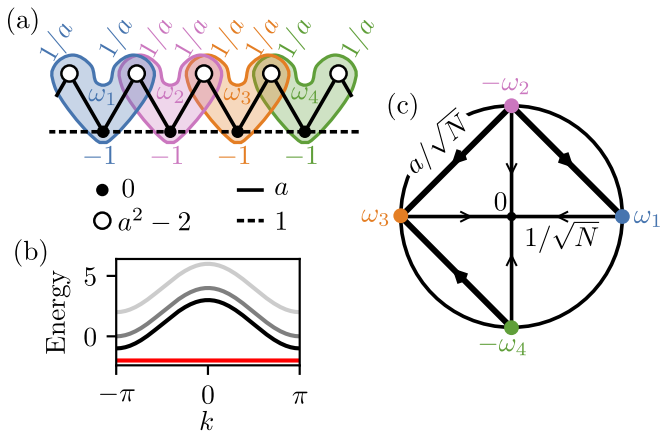


FIG. S5. (a) Sawtooth ladder with a flat band at energy  $-2$ . A possible choice of CLS is shown for each unit cell (different colors). (b) Band dispersions for  $a = 1$  (black),  $a = \sqrt{2}$  (gray) and  $a = 2$  (light gray). The flat band of interest is shown in red. (c) Example of  $\omega_i$  leading to uniform densities for  $a = \sqrt{2}$ . The CLSs are centered at a site without overlaps, which constrains  $|\omega_i| = 1/\sqrt{N}$  to achieve uniform densities. The overlaps between adjacent CLSs constrain  $|\omega_{2n\pm 1} + \omega_{2n}| = |\omega_{2n\pm 1} - (-\omega_{2n})| = a/\sqrt{N}$ , constraining the distance between  $\omega_{2n}$  and  $\omega_{2n\pm 1}$ . As a result,  $0$ ,  $-\omega_{2n}$  and  $\omega_{2n\pm 1}$  always form an isosceles triangle in the complex plane.

different normalization. There can exist no other states  $R|\varphi_0\rangle$  on the flat band.

Note that the assumption of a nonzero area is essential. If a framework consists of triangles with vanishing surface area, it generally becomes possible to construct both pairs of states  $RU|\varphi_0\rangle$ ,  $RU^\dagger|\varphi_0\rangle$ , and single problematic states  $R|\varphi_0\rangle$ .

## VII. SAWTOOTH LADDER

The sawtooth ladder, also studied in Ref. 29, is an example of a flat-band model with CLSs compatible with bosonic condensation. We consider a generalized version of the model with a tuning parameter  $a$  (see Fig. S5). This model always features a lowest isolated flat band at energy  $-2$ , and uniform-density eigenstates exist on the flat band for any  $0 < a \leq 2$ .

As shown in Fig. S5c, the CLSs in this model overlap in such a way that, for uniform densities,  $0$ ,  $-\omega_{2n}$  and  $\omega_{2n\pm 1}$  always need to form an isosceles triangle. Whenever  $0 < a < 2$ , uniform-density flat-band eigenstates are then represented by triangulated frameworks with nonzero area. This includes the usual flat-band sawtooth model with  $a = \sqrt{2}$ . The area of the triangles vanishes for  $a = 0$  and  $a = 2$ . At  $a = 0$ , the instability of condensation is evident: the flat band is then completely trivial (it arises from completely disconnected lattice sites). At  $a = 2$ , condensation is expected to be impossible due to the existence of problematic flat-band eigenstates, similarly to

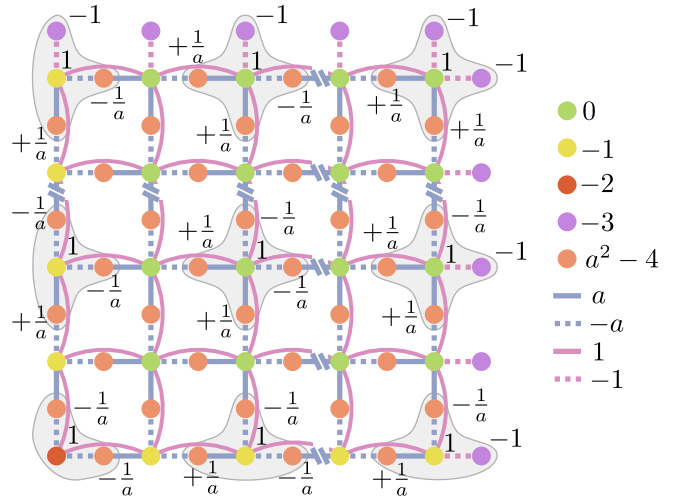


FIG. S6. Tasaki model with adjusted boundary conditions. The shaded areas represent the different types of CLSs in the system.

the Tasaki model considered in the main text.

## VIII. TASAKI FLAT-BAND MODEL

### A. Adjusted boundary conditions

The system sizes for which we can compute zero-point energies and  $n_0$  are limited, since we need to diagonalize a  $(2N) \times (2N)$  matrix. In the Tasaki lattice, uniform-density flat-band eigenstates would then be commensurate with accessible system sizes only for a few specific values of  $a$ . We therefore choose to use open boundary conditions. In order to retain a perfectly flat band and a uniform-density  $|\varphi_0\rangle$ , we modify the tight-binding parameters at the boundaries as shown in Fig. S6. In this case, the CLSs for unit cells in the bulk are unchanged, but CLSs at boundaries and corners are slightly different. However, they overlap with other CLSs in the same way as bulk CLSs would, and the mapping explained below can be used.

### B. Sampling of zero-point energies

#### 1. Correspondence between uniform-density flat-band eigenstates and 3-colorings

As mentioned in the main text, we sample uniform-density flat-band eigenstates by taking advantage of a correspondence between them and three-colorings of the square graph. For flat-band eigenstates with a uniform  $|\varphi_{i\alpha}| = 1/\sqrt{N}$ , we need  $\omega_i = e^{in\theta}/\sqrt{N}$ , where  $n$  is an integer and  $\theta = 2 \arcsin(a/2)$ , with  $a \in [1, 2)$  a tuning parameter. The phases of  $\omega_i$  and  $\omega_j$  corresponding to

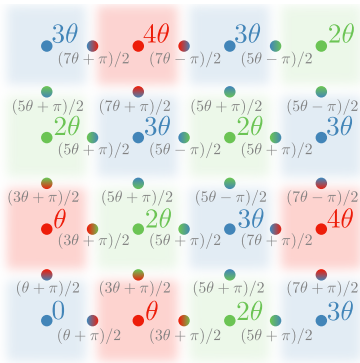


FIG. S7. Mapping between three-colorings of the square lattice and uniform-density eigenstates  $|\varphi_0\rangle$ . At each site at a corner of a square plaquette (referred to as corner site),  $\varphi_{i\alpha} = \omega_i$ , and thus the phase increases by  $\theta$  when moving from blue to red, red to green, or green to blue. Otherwise, it decreases by  $\theta$ . Once all  $\omega_i$  are known, the phases at the sites on the edges of square plaquettes (referred to as edge sites) are easy to determine.

adjacent unit cells need to differ by exactly  $\pm\theta$ . We divide the possible phases of  $\omega_i$  into three sets,  $\{0, 3\theta, \dots\}$ ,  $\{\theta, 4\theta, \dots\}$ ,  $\{2\theta, 5\theta, \dots\}$ , and associate each with a color (blue, red and green, respectively). We now color each unit cell with the color corresponding to the phase of  $\omega_i$  in that unit cell. Since the phases in neighboring unit cells need to differ by  $\pm\theta$ , neighboring unit cells always are associated to different colors: we obtain a three-coloring of the square lattice.

We can also show that each three-coloring of a square lattice corresponds to a uniform-density  $|\varphi_0\rangle$ . We start from a three-coloring of the square lattice and associate each site of the square lattice to a unit cell. Let us assume we know the phase  $\theta_i$  of  $\omega_i$  in one unit cell  $i$ , and want to determine the phase  $\theta_j$  in a neighboring unit cell  $j$ . If the colors associated with  $i$  and  $j$  are blue and red, red and green, or green and blue, respectively (“increasing” color from  $i$  to  $j$ )  $\theta_j = \theta_i + \theta$ . Otherwise,  $\theta_j = \theta_i - \theta$  (see Fig. S7). As a starting point, we can choose the phase in any unit cell, which amounts to fixing the gauge, and then determine the other  $\omega_i$  following this procedure. This will always yield a uniform-density wavefunction (where all neighboring cells differ by  $\pm\theta$ ), which can be seen by considering a group of  $2 \times 2$  unit cells. If we go around this plaquette, we need to start and end at the same color. Since we work with three colors, the only possibility is to increase the color twice and decrease the color twice. Going around the plaquette, we thus increase the phase twice, and decrease twice, meaning we are guaranteed to start and end with the same phase. Since all such  $2 \times 2$  sets need to be consistent, all phases will be consistent.

Note that three-colorings of the Tasaki lattice are also directly related to three-colorings of the square lattice (we are simply adding vertices the color of which is completely determined by the underlying square lattice), and we could

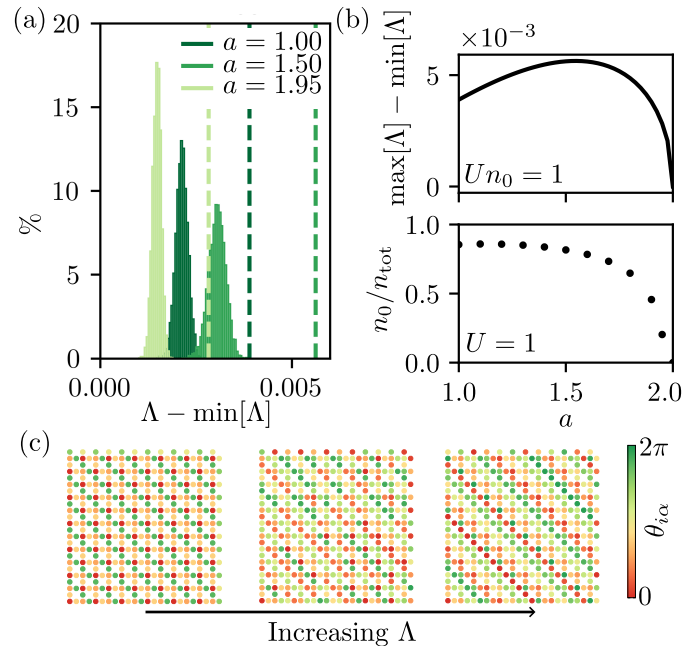


FIG. S8. (a) Zero-point energies for 5000 randomly sampled wavefunctions  $|\varphi_0\rangle$  at different values of  $a$  in the Tasaki model. The energies are shifted by the smallest ZPE,  $\min[\Lambda]$ . The dashed line indicates the highest ZPE,  $\max[\Lambda]$  for each  $a$ . We consider a system of  $12 \times 12 \times 3$  sites. We set  $Un_0 = 1$ . (b) Range of ZPEs,  $\max[\Lambda] - \min[\Lambda]$ , (upper panel) and  $n_0/n_{\text{tot}}$  assuming condensation in the state with lowest ZPE (lower panel) and as a function of  $a$ . For the computation of  $n_0$ , we set  $n_{\text{tot}} = 1$ . The lower panel is reproduced in the main text. (c) Examples of states corresponding to the lowest (left), intermediate (middle) and highest (right) ZPEs for  $a = 1.5$ . These states have uniform densities,  $\varphi_{i\alpha} = e^{i\theta_{i\alpha}}/\sqrt{N}$ .

in principle interpret the three-color sampling as three-colorings of the Tasaki lattice itself. However, it is important to stress that the mapping to three-colorings is purely reliant on constraints on phases of  $|\varphi_0\rangle$ , which are a consequence of the way CLSs overlap, rather than of the connectivity of the lattice. For any lattice with the same basis of CLSs as our Tasaki model, possible  $|\varphi_0\rangle$  could always be sampled from three-colorings of the square lattice, even when the connectivity of the actual lattice is not the same as the Tasaki lattice.

## 2. Numerical results

ZPEs for states corresponding to random three-colorings of the square graph are shown in Fig. S8a for different values of  $a$ . The total range of ZPEs,  $\max[\Lambda] - \min[\Lambda]$ , decreases rapidly when the limit  $a \rightarrow 2$  is approached (see Fig. S8b). This quantity gives an estimate of the magnitude of thermal fluctuations that would destabilize the condensate [30], and this is thus a signal that the condensate becomes increasingly unstable close to  $a = 2$ . As men-

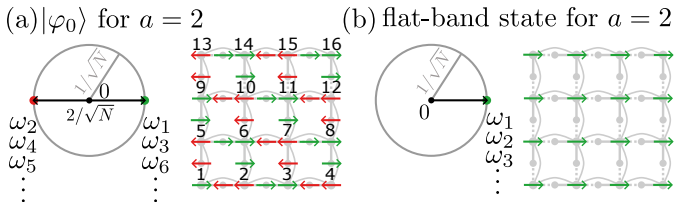


FIG. S9. (a) Bloch state at  $(\pi, \pi)$  and corresponding coefficients  $\omega_i$  in the complex plane. When  $a = 2$ , this is the only flat-band eigenstate minimizing  $E_{\text{MF}}$ . (b) Flat-band eigenstate which contributes to the destabilization of the condensate for  $a = 2$ . This state does not minimize  $E_{\text{MF}}$ , but its existence still contributes to destabilizing the condensate due to geometric effects.

tioned in the main text, this is corroborated by the condensate fraction decreasing close to this limit. The instability at  $a = 2$  is explained in more detail in Sec. VIII B 3.

Some examples of  $|\varphi_0\rangle$  corresponding to the lowest, intermediate and highest ZPEs are shown in Fig. S8c. For all values of  $a$ , we find that the states  $|\varphi_0\rangle$  with the lowest zero-point energy correspond to two-colorings of the square lattice. This means that  $\omega_i$  alternates between two values, e.g.  $1/\sqrt{N}$  and  $e^{i\theta}/\sqrt{N}$  with  $\theta = 2 \arcsin(a/2)$ .

This state corresponds to a superposition of two Bloch states. The Bloch states at  $\mathbf{k} = (0, 0)$  and  $\mathbf{k} = (\pi, \pi)$  have periodic parts  $|u_\Gamma\rangle = (1, 0, 0)^T$  and  $|u_M\rangle = (a/2, -1, -1)^T / \sqrt{2 + (a^2/4)}$ , respectively. From these states, it is possible to construct a uniform-density state  $(\sqrt{2 + (a/2)^2} |u_M\rangle e^{i(\pi, \pi) \cdot \mathbf{R}_i} \pm i\sqrt{4 - a^2} |u_\Gamma\rangle / 2) / \sqrt{3}$ , where  $\mathbf{R}_i$  is the position of the  $i$ :th unit cell. This is the superposition corresponding to two-colorings of the square lattice.

The highest zero-point energy is found for three-

colorings where the color index always increases or decreases when moving along  $x, y$ . These states correspond to the Bloch functions at  $\mathbf{k} = 2\arcsin(a/2)(\sigma, \sigma')$ ,  $\sigma, \sigma' \in \{-1, 1\}$ , which have uniform densities. In this model, the most favorable states for condensation are therefore superpositions of Bloch functions, while Bloch functions with uniform densities are the least favorable. A standard momentum-space approach would therefore consider condensation in the least favorable uniform-density state, except if the unit cell is enlarged.

### 3. Instability of condensation for $a = 2$

As shown in the main text, bosonic condensation becomes unstable in the Tasaki lattice when approaching  $a = 2$ . At  $a = 2$ , the distance between coefficients  $\omega_i$  corresponding to overlapping CLSs needs to be  $2/\sqrt{N}$  for uniform densities. Since the coefficients are all on the same circle of radius  $1/\sqrt{N}$ , they need to be diametrically opposed: there is only one  $|\varphi_0\rangle$  minimizing the mean-field energy (excluding gauge transformations), shown in Fig. S9(a). This is the Bloch state at  $(\pi, \pi)$ . Because there is no degeneracy in the minimization of  $E_{\text{MF}}$ , we could naively expect the condensate to be more stable than at  $a < 2$ , not less.

However, the issue here is the existence of a multitude of non-uniform flat-band eigenstates relating to  $|\varphi_0\rangle$  by  $|\varphi'_0\rangle = R|\varphi_0\rangle$  (one example is shown in Fig. S9(b)). In the complex plane, if we do not require uniform densities, we can move every coefficient  $\omega_i$  continuously along the diameter of the circle without adding complex phases to any  $\varphi_{i\alpha}$ . While the framework consists of only triangles with 0 and two coefficients  $\omega_i$  as their vertices, the area of the triangles vanishes, and stability is no longer guaranteed.